



# A Review on Monitoring of Organic Pollutants in Wastewater Using Electrochemical Approach

Azeez Olayiwola Idris<sup>1,2</sup> · Benjamin Orimolade<sup>3</sup> · Lynn Dennany<sup>4</sup> · Bhekile Mamba<sup>3</sup> · Shohreh Azizi<sup>1,2</sup> · K. Kaviyarasu<sup>1,2</sup> · Malik Maaza<sup>1,2</sup>

Accepted: 9 June 2023 / Published online: 17 July 2023  
© The Author(s) 2023

## Abstract

This review focuses on monitoring selected organic contaminants utilising an electrochemistry technique due to intrinsic benefits such as simplicity, portability, cost, and improved sensitivity. Because the presence of organic pollutants in water causes a variety of health issues such as tumour, headaches, tiredness, and developmental abnormalities, it is critical to explore an effective approach to quantifying these contaminants in various matrices. Although remarkable results have been documented in the use of conventional techniques in the quantification of organic pollutants, owing to high costs, longer pre-concentration steps and analysis times, high power consumption, and the need for sophisticated skilled personnel, their applications for monitoring organic pollutants on-site have been hampered. The electrochemistry approach has emerged to address the difficulties that have hindered the use of traditional approaches for quantifying organic contaminants in water. Thus, the purpose of this review is to examine the concept of employing electrochemistry techniques to determine organic contaminants in various matrixes, and various recommendations for future research have been highlighted.

**Keywords** Nanomaterials · Electrodeposition · Electropolymerisation · Organic pollutants · Sensor · Electrodes · Immobilisation · Aptasensors

## Introduction

The ongoing pollution of water sources as a result of industrial growth and development has caused major environmental concerns due to the negative consequences on plants, animals, and humans [1, 2]. Some of these organic compounds are released into the water bodies because they are employed

in various applications [1, 2]. For example, chlorophenols have been utilised for many years in a variety of applications such as insecticides, wood preservation, herbicides, and anti-septics [3]. Bisphenol A (BPA), an endocrine disruptor, is utilised in the manufacture of polycarbonate and epoxy coatings [4, 5]. Hydroquinone, on the other hand, is employed in a variety of industries, including cosmetics, food technology, chemistry, and pharmaceuticals, to mention a few [6, 7].

Numerous studies have found that excessive levels of organic contaminants in water cause a variety of health issues, including headaches, renal damage, exhaustion, nausea, tumours, tachycardia, and developmental difficulties [8, 9]. As a result, the US Environmental Protection Agency (USEPA) has classified several organic pollutants, including bisphenol A, chlorophenols, and hydroquinone, as main pollutants [10–12], necessitating strong and portable detection methodologies for environmental monitoring.

BPA was found in 75% of 45 canned beverages tested in Belgium, ranging from 0.02 to 8.1 gL<sup>-1</sup> [12]. Similarly, in Italy, BPA was found in 100% of milk-based beverages and 50% of carbonated beverages [12]. Furthermore, a French study found that BPA levels in 176 different composite foods

✉ Azeez Olayiwola Idris  
idrisalone4real@gmail.com

<sup>1</sup> Nanoscience and Nanotechnology College of Graduates Studies, UNESCO-UNISA Africa, University of South Africa, Pretoria 392, South Africa

<sup>2</sup> Nanosciences African Network (NANOAFNET), iThemba LABS-National Research Foundation, Somerset West, 7129, Western Cape, South Africa

<sup>3</sup> Institute for Nanotechnology and Water Sustainability (iNanoWS), College of Science, Engineering and Technology, University of South Africa, Florida Science Campus, Private Bag X6, Johannesburg 1709, South Africa

<sup>4</sup> WESTChem Department of Pure and Applied Chemistry, Technology and Innovation Centre, University of Strathclyde, 99 George Street, Glasgow, UK

ranged from 0.105 to 28.370 g kg<sup>-1</sup> [12]. As a result, France banned the use of BPA in food matrixes in 2015 [12]. Due to this, we report a review of the detection of BPA in various matrixes.

Today, chemiluminescence, liquid chromatography–mass spectrometry, high-performance liquid chromatography, capillary, gas chromatography, and fluorimetry are used for POP environmental monitoring [13–18].

Conventional analytical methods for the detection of organic pollutants in environmental samples are generally based on separation by chromatographic techniques. Furthermore, many different detection principles are currently associated with both liquid (LC) and gas chromatography (GC). However, mass spectrometry (MS) is, by far, the most used detection platform for environmental screening purposes. This is mainly due to its high selectivity, specificity, and sensitivity, and also its capability of delivering structural qualitative data of the analytes in the study, aiding to overcome undesired matrix interferences [16].

Different chromatographic separation (GC and LC) and MS detection platform combinations are used in the monitoring of organic pollutants in various matrixes, providing a variety of options for scientists to use by their objectives. These analytical methods have been thoroughly investigated as a tool for environmental analysis, ranging from GC–MS to high-resolution liquid chromatography quadrupole time-of-flight mass spectrometry (LC-Q-TOF–MS) and ultra-high pressure liquid chromatography with tandem mass spectrometry (UHPLC-MS/MS) [13–18]. Furthermore, given the capability of multi-residue identification provided by high-resolution mass spectrometry (HRMS) techniques, several approaches, such as targeted, suspicious, and non-targeted screening, may be chosen when it comes to environmental screening for organic pollutants [16]. These analytical techniques are distinguished by their high accuracy, precision, and low detection limits [19]. However, the disadvantages of these methods include high costs, longer pre-concentration steps and analysis times, high power consumption, and the need for sophisticated skilled personnel, with some having limited potential for portable detection [20]. As a result, there is a drive to develop detection strategies with low power consumption, high sensitivity, fast response time, and portability for on-site monitoring of toxic POPs in the environment.

Due to its simplicity, portability, affordability, and superior sensitivity, the electrochemical approach is a good candidate to overcome the drawbacks of traditional techniques. In electrochemistry, the sensor employed for the electrochemical analysis is the electrodes, nanomaterials, and the analyte of interest. Sometimes, the nanomaterials are not even incorporated into the sensor development but to obtain a low detection limit, nanomaterials are incorporated in the sensor fabrication processes. Electrochemical approaches

have provided novel opportunities for the detection of biological molecules [21–24], illegal substances, heavy metals [20, 25], and organic pollutants [26, 27]. This method can also take advantage of smart nanomaterials, which allow for quicker electron transit, better conductivity, and quantum effects to improve sensitivity and selectivity within complicated matrices [28, 29]. It is vital to note that BPA is electro-oxidised by two protons and two electrons at the electrode-solution interface. As a result, the electrochemistry technique is used for BPA detection.

Bisphenol A is an endocrine-disrupting compound (EDC) that has estrogenic activity even at low concentrations of less than 1 ngL<sup>-1</sup> [12]. It is concerning to note that 90% of the world's population, including infants, has residues of bisphenol A in blood and urine in concentrations ranging from 0.32 to 2.5 ng mL<sup>-1</sup> and from 0.11 to 946 ng mL<sup>-1</sup>, respectively. [12]. Furthermore, it has been reported that BPA is present in a variety of foods (fruits, meat, vegetables, cereals, composite meals, pasta, milk, and dairy products sold in the EU) [12]. As a result, BPA was included in this review's list of harmful contaminants.

HQ pollution is also becoming a more important global issue, with the potential to cause extensive harm to human health via cutaneous, oral, and respiratory routes [12]. Both the US Environmental Protection Agency (EPA) and the European Union (EU) have listed both HQ and nitrophenol on their lists of priority pollutants to be monitored in the aquatic environment [2, 11]. Thus, this review focuses on the application of smart nanomaterials for the electrochemical detection of carefully selected toxic organic pollutants, including bisphenol A, hydroquinone, and 4-nitrophenol.

## Sensing of Bisphenol A (BPA)

Bisphenol A (BPA) is used in the manufacturing of a variety of consumer goods, including nursing bottles, food cans, flame retardants, tableware, dental fillings, and beverage containers [30, 31]. BPA is an endocrine disruptor, and even 1 mg/L exposure through food and water can be harmful to human health [32, 33]. BPA in the blood causes a variety of health issues, including recurrent miscarriages, reproductive dysfunction, polycystic ovarian syndrome, cancer, diabetes, endometrial hyperplasia, and aberrant karyotypes, among others [34, 35]. BPA binds to oestrogen receptors at low doses (100 pM), causing chronic illnesses, reproductive problems, cancer, and diabetes [36]. The European Food Safety Authority mandated in 2015 that the tolerated daily intake of BPA be set at 0.004 mg/L [36]. Because BPA is non-biodegradable and highly resistant to chemical degradation, it is critical to monitor its content in the environment [36]. Jemmeli et al. created a low-cost paper-based electrochemical sensor for BPA measurement using carbon-black-modified ink (Fig. 1). [37]. This platform was used to

**Fig. 1** The fabrication of eco-friendly devices for the detection of BPA in river water (reproduced with permission from Copyright Elsevier Ref. [37])



identify the presence of BPA in river water. The described paper-based electrochemical sensor was inexpensive, portable, and easy to use, with sample flow achieved without the use of external pumps.

Similarly, carbon black was immobilised on a screen-printed carbon electrode (SPCE) along with gold nanoparticles and magnetic imprinted polymer for the detection of BPA in tap and mineral water samples [38]. The scan rate studies demonstrated that the electrochemical oxidation of BPA on the designed electrode was controlled by adsorption and was irreversible. The author's findings demonstrated that as the scan rate increased, the value of anodic peak potential altered positively. The author underlined that, under optimal experimental conditions, differential pulse voltammetry (DPV) was more sensitive to BPA detection than square-wave voltammetry (SWV). As a result, it was utilised to detect BPA. We hypothesise that the different detection limits reached by both approaches are due to the electrode and modifier composition. The detection limit of  $0.0088 \mu\text{M}$  was reported [38] when carbon black@AuNPs@MIP (carbon black@gold nanoparticles@molecularly imprinted polymer) was employed as a modifier, which is lower than the detection limit of  $0.03 \mu\text{M}$  achieved when carbon black was used [37]. All of the modifiers' synergistic effects, including carbon black@AuNPs@MIP, are responsible for the considerable improvement in the detection limit.

An electrochemical sensor for BPA was developed using the synergy of reduced graphene oxide (rGO) and carbon nanoparticles (CNPs) [39]. The electrochemical responses of the modifiers were investigated using cyclic voltammetry (CV), and the results revealed that GCE/CNPs@rGO provided the best electrocatalytic response, followed by GCE/CNPs and GCE/rGO. Given this, the electrocatalytic determination of BPA on the electrode occurred due to the existence of quantum confinement on the CNPs, which serves as a proton source, and the carbon atom oxygenated groups (C–O, C=O, and O–C=O) on the rGO, which serves as

a proton source. To prepare carbon nanoparticles, we purpose using various synthetic techniques (co-precipitation, solvothermal, and sol–gel) and precursors. This is due to the economic considerations, which raise the sensor's price, as well as the fact that different precursors create variable amounts of the final product. Certain precursors like sodium borohydride and hydrogen cyanide are exceedingly dangerous and must be avoided at all costs. In comparison to earlier sensors, there was a significant improvement in the detection limit [38]. The improved detection limit of BPA was due to the superior conductivity of carbon analogue combination. It is also critical to utilise a variety of reducing agents to convert graphene oxide to reduced graphene, particularly eco-friendly reducing agents such as ascorbic acid and fruit extracts, to limit the chance of researchers being exposed to toxic compounds that can affect their respiratory systems. The author was able to successfully reduce GO to rGO utilising CNPs in a one-pot synthesis, but the chemistry of the two modifiers employed for sensor fabrication was not disclosed. The issue with this approach in our assessment is that it makes comparing the electrochemical performance of each modifier difficult, which is required for a proof-of-concept study.

A three-dimensional hierarchical cylinder-like nickel nanoparticle@nitrogen-doped carbon nanosheet@chitosan nanocomposite (NiNPs@NCN@CS) was used to modify GCE for the detection of BPA [40]. Pyrolysis of nickel-1,3,5-benzene tricarboxylic acid metal–organic frameworks under a nitrogen atmosphere yielded the nickel nanoparticle@nitrogen-doped carbon nanosheet. The nanocomposite demonstrated good electrical conductivity, robust electrocatalytic activity, and a large surface area, all of which contributed significantly to the sensor's sensitivity and reproducibility. Due to the creation of electroactive p-benzoquinone and o-benzoquinone as by-products during the electro-oxidation of BPA, the sensor was reported to have significant anti-fouling properties. The author claimed

that NiNPs and chitosan were responsible for the sensor's anti-fouling characteristics. We urge that researchers investigate the chemistry of interaction that occurs when many modifiers are utilised in sensor development; this will aid in understanding the chemistry of interaction between the modifiers and the analyte.

For the detection of BPA, unique electrochemical molecularly imprinted polymers (MIPs) were wired on the surface of a screen printed carbon electrode [41]. The redox tracer/functional monomer ferrocenyl methyl methacrylate was inserted into the binding cavities of a cross-linked molecularly imprinted polymer. Because of their simplicity of synthesis, great promise as a stable recognition element, high stability, low cost, strong selective recognition properties, and ability to behave as “plastic antibodies,” MIPs are being used in sensor design. The sensor detected BPA at a value of 0.06 M. The author's employment of CV methods, which are less sensitive than SWV and DPV, contributed to the platform's high detection limit when compared to previously reported sensors [38]. Notwithstanding the authors' success in imprinting the polymer on SPCE, we believe that an electrodeposition approach would be preferable because the voltage is employed to immobilise the nanomaterials on a conducting substrate. As a result, the modifier's stability improves, and the outcome can be easily reproduced using this method. Unfortunately, the majority of investigations used a drop-drying approach, which causes modifiers to leak into the analytical solution after only a few runs, resulting in inconsistent results and an unstable sensor. We hypothesised that this was one of the reasons why most electrochemistry sensor technologies have yet to be commercialised.

Anirudhan and colleagues developed non-imprinted polymer (NIP) and MIP, with the latter demonstrating greater stability and repeatability in the detection of BPA [42]. The author argued that the lower response of NIP compared to MIP was due to a lack of imprinting sites and low electrocatalytic activity, while the presence of complementary cavities was thought to be responsible for the MIP/improved GCE's redox response. The fabricated sensor (MIP/GCE) detected BPA at concentrations as low as 0.02 M and was utilised to detect BPA in extracts from baby feeding bottles. Similarly, MIP was introduced into the matrix of graphene quantum dots (GQDs) for the detection of BPA in the sea and tap water samples [43]. The sensor was prepared by dropping GQD solution on the surface of GCE and allowed to dry at ambient temperature. Thereafter, MIP was electropolymerised on the surface of GCE/GQDs by cycling a potential from  $-0.2$  V to  $0.8$  V at a scan rate of  $100$  mV/s using CV. The sensor was stable and showed excellent reproducibility which was accredited to the remarkable stability of the modifier and the reversibly binding of the imprinted sites to bisphenol A. It is essential to highlight that the author mentioned that the detection process did not involve the

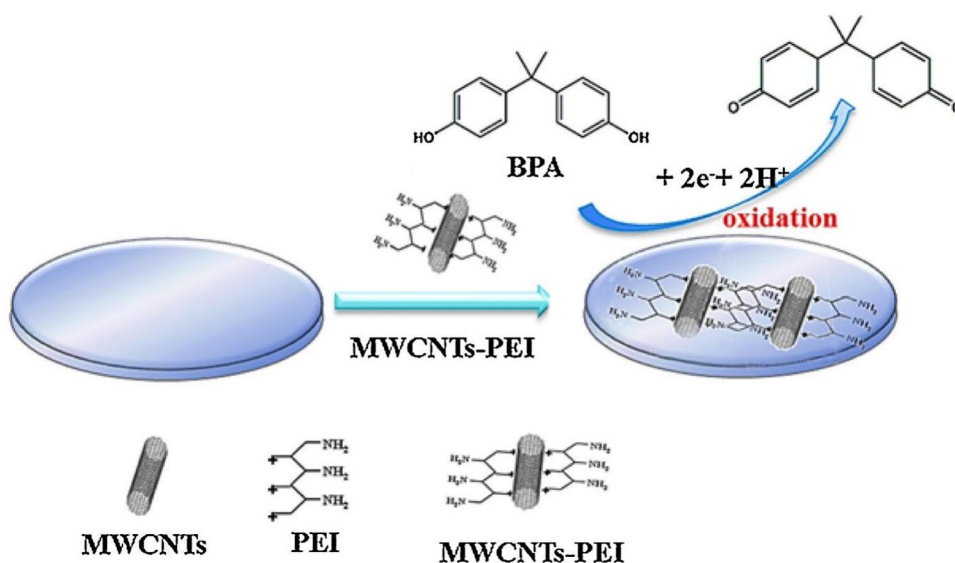
oxidation reaction of BPA, but the polymerisation of MIP/QDDs on GCE.

Ionic liquid has recently been used in the development of sensors due to its unique analytical properties, which include high ionic conductivity, a large potential window, and exceptional chemical stability [44]. As a result, Butmee et al. employed ionic liquid (1-butyl-2, 3-dimethyl imidazolium tetrafluoroborate) functionalised graphene nanoplatelets (FGN) for BPA measurement [45]. The ionic liquid not only improved the electrochemical performance of the FGN, but it also helped to disperse the FGN on the electrode surface by providing a surface charge. The ionic liquid can be used as a dispersion agent to aid in the immobilisation of nanomaterials on conducting substrates. The charge on the surface of an ionic liquid, in our opinion, aids in the migration of the analyte onto the electrode surface.

Black phosphorus (BP) functionalised porous graphene (PG) was used as a platform for the electrochemical detection of BPA [46]. The key to effectively synthesising the porous graphene functionalised black phosphorus composite, also known as PG-BP, was a strong coherent coupling between porous graphene surface plasmons and anisotropic black phosphorus localised surface plasmons. This was accomplished with the use of infrared drying and penetrating infrared radiation. The electrochemical effective surface area (ESA) of the modifiers was interrogated using chronocoulometry by the Anson equation. Since different electrochemical methods for detecting analytes have different sensitivities, it is important to employ a variety of them. The ESA of the glassy carbon electrode (GCE) was  $0.016$  cm<sup>2</sup> and  $0.090$  cm<sup>2</sup> for GCE-PG@BP. The results obtained confirmed that the modifier enhanced the surface area of the electrode and was successfully used for the detection of BPA in food packaging and urine. It is important to highlight that the surface area of the conducting substrate plays a pivotal role in the detection limit of the analyte with the understanding that the enhancement of the electrochemically effective area of the GCE is beneficial to the concentration of the substance on the electrode surface, and it also improves the electrochemical response signal of substance.

A sensor for BPA detection was developed using multiwalled carbon nanotubes (MWCNTs) and polyethylene imine (PEI) [47]. The sensor was constructed by sonicating a mixture of MWCNTs and PEI solutions for 10 min and then oscillating for 120 min. The resultant solution was thoroughly filtered and rinsed with ultra-pure water. Following that,  $8$   $\mu$ L of MWCNTs-PEI was drop dried on the GCE surface to form the sensor employed in the detection of BPA. The scan rate studies revealed that the electrochemical oxidation of BPA in the constructed sensor (MWCNTs/PPI@GCE) is a two-electron and two-proton process, as shown in Fig. 2. The sensor has an outstanding electrocatalytic capability for detecting BPA, which was attributed to

**Fig. 2** Schematic view of the electrochemical sensor prepared from MWCNT-PEI composites (reproduced with permission from Copyright Elsevier, Ref. [47])



the MWCNTs' superior conductivity and the positive charge of the PEI, which allowed electron transfer/loading of the BPA on the electrode surface. The author, in our judgement, used MWCNTs and PEI based on the electrostatic attraction between the negative charge particles of the MWCNTs and the positive charge of the PEI. It is important that for future studies, the PEI should be electrodeposited separately on the electrode surface and MWCNTs should be dispersed separately in dimethyl formamide (DMF); this will make it easier to compare the conductivities of the two modifiers.

Ali and his colleagues designed an electrochemical sensor for BPA measurement using MWCNTs and cyclodextrin (BCD) (Fig. 3) [48]. By using one-step Steglich

esterification, the modifiers were networked on the surface of a SPCE. The measurement of BPA indicated an irreversible mechanism involving two protons and two electrons in a diffusion-controlled oxidation. The sensor's excellent sensing capability was attributed to the host-guest interaction capacity of MWCNTs-BCD with the analyte, combined with BCD's hydrophilic behaviour and large surface area of the modifiers. The sensor remained stable for more than 5 weeks, according to the author, and an excellent recovery rate of 96.05–108.7% was obtained. Because of the nature of the conducting substrate, the sensor was stable from our perspective (SPCE). The electrode was not dropped inside the analyte solution; instead, the analyte and modifiers were

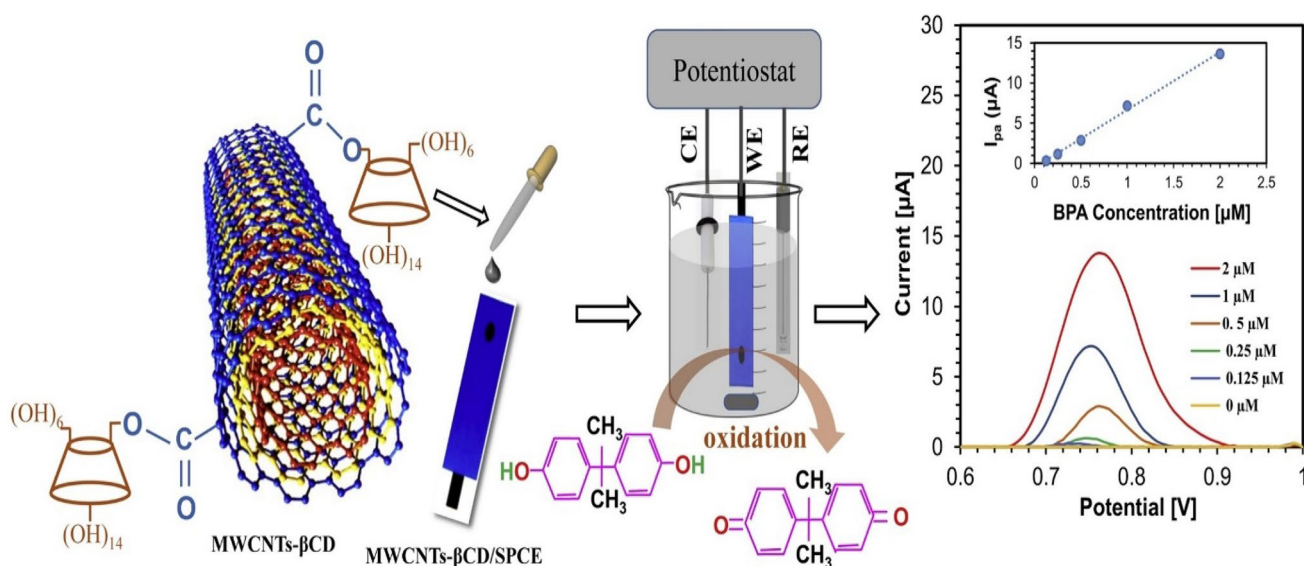


**Fig. 3** The systematic scheme for the sensor fabrication using MWCNTs-BCD (reproduced with permission from Copyright Elsevier, Ref. [48])

carefully dropped on the surface of the SPCE before electrochemical measurement. SPCE should be the electrode of choice for electrochemical analysis because of its design, which provides a comfortable environment and interaction between the modifiers and analyte. Unlike, for example, GCE, carbon paste electrodes, and exfoliated graphite electrodes to name a few.

For the measurement of BPA, a gold nanoparticle (AuNP) was electrodeposited on MIP together with binary functional monomers (4-amino thiophenol (4-ATP) and chitosan (CS)) [49]. Electrodeposition of AuNPs on 4-ATP in the presence of chitosan produced the molecularly imprinted sensor. According to the author, the UV data revealed an intermolecular force between the amino group of 4-ATP molecules and the –OH group of BPA, which was critical in the creation of BPA molecular recognition sites in the BPA MIP. Surprisingly, the author used an electrodeposition method for the sensor development, which improved sensor stability. With a recovery rate of 97.6–106.5%, the sensor was successful in detecting BPA in milk and plastic samples. It is critical to emphasise that the electrodeposition method is one of the best modification routes for stabilising modifiers on the surface of a conducting substrate.

MWCNTs and gold nanoparticles were annexed together to develop an impedimetric sensor [50]. The MWCNTs were functionalised with nitric acid to incorporate the carboxylate functional group, which aids in the loading of more BPA onto the electrode surface. Various weights of functionalised MWCNTs were dispersed in 100  $\mu\text{L}$  of 1.0% chitosan solution (0.05, 0.1, 0.2, 0.5, and 1 mg). According to the findings of the study, when 0.5 and 1 mg of BPA were employed for voltammetric detection, the background current was noisy, and the reaction to BPA was noticed at higher doses. As a result, for the sensor development, 0.2 mg MWCNTs was employed with five drops of AuNPs on the electrode surface. After 4 weeks, the sensor preserved 85% of its initial reactions, confirming the promising stability of the AuNPs/MWCNT/GCE. Indeed, the author employed three, five, and seven drops of AuNPs, with the results confirming that five drops provided the best electrochemical signal. We hypothesised that five drops produced the strongest electrochemical signal because a higher drop might cause the AuNPs to agglomerate and could limit electron mobility, which will invariably affect the sensor performance. The author employed DPV and impedimetric electrochemical techniques to detect BPA. For future studies, at least two electrochemical techniques should be utilised to quantify an analyte; this will help to validate the results acquired from both approaches and confirm the optimal methodology for analyte detection.

A label-free electrochemical aptasensor for BPA was developed using functionalised MWCNTs and gold nanoparticles [51]. The aptamer was wired onto the *f*-MWCNTs@

AuNPs nanocomposite via thiol-gold (S–Au) linkages formed by the interaction of the Au and sulphur atoms in the aptamer. A molecular dynamic (MD) simulation was used to investigate the interaction/chemistry between the aptamer and the BPA. Because of the aptamer molecules' great affinity for BPA, high conductivity, and vast surface area of the *f*-MWCNTs@AuNPs nanocomposite, the aptasensors detected BPA down to 0.05 nM. It is critical to emphasise that due to the aptamer's strong affinity for BPA, the aptasensor method is an excellent concept for overcoming the interference issues encountered during BPA sensing. Similarly, a label-free electrochemical determination of BPA in milk samples was fabricated by decorating graphene on gold nanoparticles. The average recovery rate of 105% was obtained for the quantification of BPA in milk samples [52].

For the quantification of BPA in tap and saltwater samples, a molecularly imprinted polypyrrole (MIP-Ppy) was integrated into a matrix of graphene quantum dots (GQDs) [43]. The sensor was prepared by dropping GQD solution on the surface of GCE and allowed to dry at ambient temperature. Following that, MIP was electropolymerised on the surface of GCE/GQDs using a CV to cycle a potential from –0.2 to 0.8 V at a scan rate of 100 mV/s. The sensor was stable, and high repeatability results were recorded; this is ascribed to the modifier's remarkable stability, as well as the reversible binding of the imprinted sites to BPA. The beauty of this platform, from our perspective, is that the polymerised MIP on the GCE/GQDs prevented the GQDs from leaching within the analyte solution. This method is a clever idea for preventing modifier leaching in electroanalytical solutions. As a result, MIP played a critical role in the sensor's stability and repeatability, which is superior to the majority of the techniques utilised in the fabrication of BPA sensors.

Innovative dual-signalling aptasensors were designed for the determination of BPA [36]. The aptasensors were prepared by the electrodeposition of AuNPs on the surface of a GCE, followed by the immobilisation of 0.5  $\mu\text{M}$  bisphenol A aptamer on the surface of AuNPs/GCE by Au–S interaction for half a day. Thereafter, 1.0 mm 6-mercapto-1-hexanol (MCH) was used to block the remaining active sites of the nanomaterials against non-specific adsorption of the aptamer. Finally, the complementary DNA (cDNA) was immobilised on the MCH/aptamer@AuNPs to form the aptasensors. The fabricated sensor was incubated with different concentrations of BPA from 0.001 to 1 nM and a detection limit of 0.041 pM was obtained. The authors used a detection probe (biotin-labelled cDNA) to capture the avidin-HRP-AuNP nanoprobe via biotin-avidin specific binding, resulting in a reduced detection limit compared to the aptasensors created before [50]. The aptamer/BPA contact caused the aptamer/cDNA duplex to dissociate, allowing the cDNA to be liberated from the sensing interface and

“turn on” the BPA signal. As a result, the detection limit improved noticeably. It is critical to note that this sensor is extremely stable due to the Au–S connection produced by the gold and aptamer. An aptasensing strategy could be a good way to avoid electrode fouling by most organic contaminants during sensing.

Razavipnah and his co-workers synthesised MWCNTs-SiO<sub>2</sub>@Au core shell for the development of electrochemical aptasensors for the quantification of BPA [53]. The ferri/ferrocyanide was used as a label-free redox probe and the immobilised aptamers remain unfolded in the absence of BPA molecules. But when BPA was added, there was an interaction between the aptamer and the analyte, which was validated by a reduction in the electrochemical signal. The aptasensor was successfully used in the detection of BPA in food samples [53].

For the detection of BPA in teethers and baby bottles, poly-cetyltrimethylammonium bromide (CTAB) and MWCNTs were electropolymerised onto the surface of a pencil graphite electrode (PGE) [54]. PGE was immersed in a solution containing CTAB and carboxylic acid functionalised MWCNTs to create the sensor. Using cyclic voltammetry, the modifier was electropolymerised on the PGE by cycling a voltage between –0.8 and 1.2 V for 10 cycles at a scan rate of 100 mV/s. The sensor was sensitive to a wide range of BPA concentrations from 2 to 808 nM, and square wave voltammetry revealed a limit of detection of 134 pM. The co-electrodeposition strategy used in combining the CTAB and MWCNTs is unique to this work, as it prevents both modifiers from leaching into the analyte solution. The detection limit obtained utilising poly(CTAB)@MWCNTs/PGE was superior to MWCNT-SiO<sub>2</sub>@Au@GCE. In our opinion, the PGE used in the sensor fabrication might have contributed to the improved detection limit, with the understanding that various electrodes have different conductivities.

In other research, aptamer functionalisation on nanoporous gold film (NPGF) was used to detect BPA levels in human serum [55]. The NPGF was made by adding nitric acid to Au/Ag alloy leaves, which changed colour from silver-white to golden due to the elimination of Ag from the alloy. The built aptamer/NPGF@GCE sensor detected BPA in spike-serum samples with a recovery rate ranging from 98.9 to 100.8%. Another group was successful in reducing graphene (rG) on the surface of poly-cyclodextrin (PBC) to construct a BPA electrochemical sensor [56]. The assay approach was based on the possibility of a host–guest interaction between the PBC/rG probe and rhodamine (Rh) or the analyte. Hummer’s method was used to prepare graphene oxide (GO), which was then dispersed in PBS to generate a GO suspension. The rG was immobilised on the GCE by cycling a potential from –1.5 to 0.6 V for 25 cycles at a scan rate of 25 mVs<sup>–1</sup>. The detection limit obtained for BPA was reduced due to the synergistic effect of rG’s high

surface area and superior electron transport properties, as well as the PBC’s host–guest recognition properties. The in situ electrochemical reductions of GO on the surface of PBC, in our opinion, were the work’s stability and innovation; this strategy is environmentally friendly because it avoided the use of hazardous reagents (sodium borohydride or hydrazine), which are often used to reduce GO to rGO. In our opinion, the stability and novelty of this work were the in situ electrochemical reductions of GO on the surface of PBC; this approach is environmentally friendly because it avoided the use of hazardous reagents (sodium borohydride or hydrazine), which are often used to reduce GO to rGO.

Zhuo and his colleagues decorated graphene oxide (GO) and porous-cyclodextrin polymer on AuAgPt ternary alloy nanocrystals for simultaneous detection of BPA and bisphenol S [57]. The sensor combines the synergy of porous-cyclodextrin’s particular adsorption capacity, the amazing catalytic capacity of AuAgPt nanocrystals, and the astonishing conductivity of GO. As a result, it was used for the simultaneous detection of BPA and bisphenol S at concentrations ranging from 0.0020 to 0.00027 μM. Although the sensor provided an impressive detection limit, it is excessively expensive due to the cost dimension of precious metals utilised in the sensor design, which will ultimately inhibit commercial usage. As a result, researchers should consider the cost dimension of the modifier(s) employed in sensor construction.

A covalent organic framework (COF) electrochemical sensor was used for the co-detection of BPA and bisphenol S [58]. The sensor was constructed by sonicating mixtures of 5 mg COF, 5 mL ethanol, and 1% Nafion-ethanol solution for 120 min. Thereafter, the resulting solution was dropped and dried on the GCE at ambient temperature to remove the solvent. The electrochemical active surface area of the COF/GCE was calculated to be 0.233 cm<sup>2</sup>, which is more than the 0.195 cm<sup>2</sup> obtained for the GCE. The DPV was employed in the determination of BPS and BPA, and the oxidation peaks of the analytes were +0.812 V and +0.512 V, respectively. The sensor has an acceptable detection limit and satisfactory repeatability. The precision and stability of the sensor were associated with the Nafion used during the sensor fabrication, which helps to prevent the leaching of the modifier inside the analyte solution.

A ruthenium 2,2′-bipyridine [(Ru-bpy)<sub>3</sub>]<sup>2+</sup> was immobilised on indium tin oxide (ITO) as a catalyst for the detection of BPA [59]. The BPA was detected by monitoring the peak current of [(Ru-bpy)<sub>3</sub>]<sup>2+</sup>-BPA complex. The detection limit of BPA obtained was higher than the result obtained from gas chromatography–mass spectrometry. The sensor has the advantage of low-cost and simple operation over the analytical method. Similarly, a novel nanocomposite composed of ruthenium nanoparticles (RuNPs), graphitic carbon nitride (GCN), and polyaniline

(PA) was used in the development of an electrochemical sensor for the detection of BPA (Fig. 4) [60]. The nanocomposite was prepared by the ultrasonication method, and the fabricated sensor was used to detect BPA in animal and human samples with a wide linear range (0.1–1.1  $\mu\text{M}$ ), a detection limit of 180 pM, and sensitivity of  $1.6025 \mu\text{A} \mu\text{M}^{-1} \text{cm}^{-2}$  were reported.

$\text{TiO}_2$  was synthesised by Si et al. for photo-assisted electrochemical detection of BPA.  $\text{TiO}_2$  was surface engineered via an inorganic-framework molecularly imprinting (MI) site to customise its shape, crystal structure, and size [61]. The sensor was developed by dip-coating indium tin oxide (ITO) electrode in an ethanolic solution of MI- $\text{TiO}_2$  and oven dried at  $120^\circ\text{C}$ . The constructed electrode was used as electrochemical and photochemical catalysts. After each measurement, the fouled electrode sensor was photochemically renewed by UV illumination for half an hour in distilled water with magnetic stirring at 500 rpm. The result showed that the sensor had an outstanding detection limit and impressive stability for quantifying BPA in water samples.

The mechanism and the reaction that occurred during the photoelectrochemical detection are shown in Fig. 5.

Table 1 shows the various platforms employed for the electrochemical detection of bisphenol A.

## Sensing of Hydroquinone (HQ)

Hydroquinone (1,4-benzenediol) is a phenolic compound that is widely utilised in a variety of industrial applications such as pharmaceuticals, pesticides, antioxidants, photostabilisers, cosmetics, plastics, antioxidants, medications, dye, textiles, and oil refinery [62–64]. Industrialisation and urbanisation are increasing the sources of hydroquinone and environmental contamination in our ecosystem. As a result, HQ exposure can cause skin inflammation, vomiting, hypoesthesia, oedema, nausea, melanocyte destruction, irritative dermatitis, and mortality [65]. Large concentrations of HQ are found in cosmetics to promote high bleaching capacity; however, long-term treatment can cause skin damage. Because of the toxicity and negative consequences of HQ, the USEPA and the European Union (EU) have included 1,4-benzenediol in their list of hazardous water contaminants [66]. As a result, it is critical to monitor the concentrations of HQ in the environment.

As a result,  $\text{Co}_3\text{O}_4$  nanopowder was successfully employed to detect HQ in industrial waste effluents, extract from PVC-food packaging bags, PC-water bottles, and infant bottles [66]. The  $\text{Co}_3\text{O}_4$  nanopowder was prepared through the combustion method burning using ethylene-urea as a novel fuel. A thin film coating of  $\text{Co}_3\text{O}_4$  nanopowder

**Fig. 4** The scheme for the synthesis of nanomaterials used for the detection of BPA in human and animal samples (reproduced with permission from Copyright Elsevier, Ref. [60])

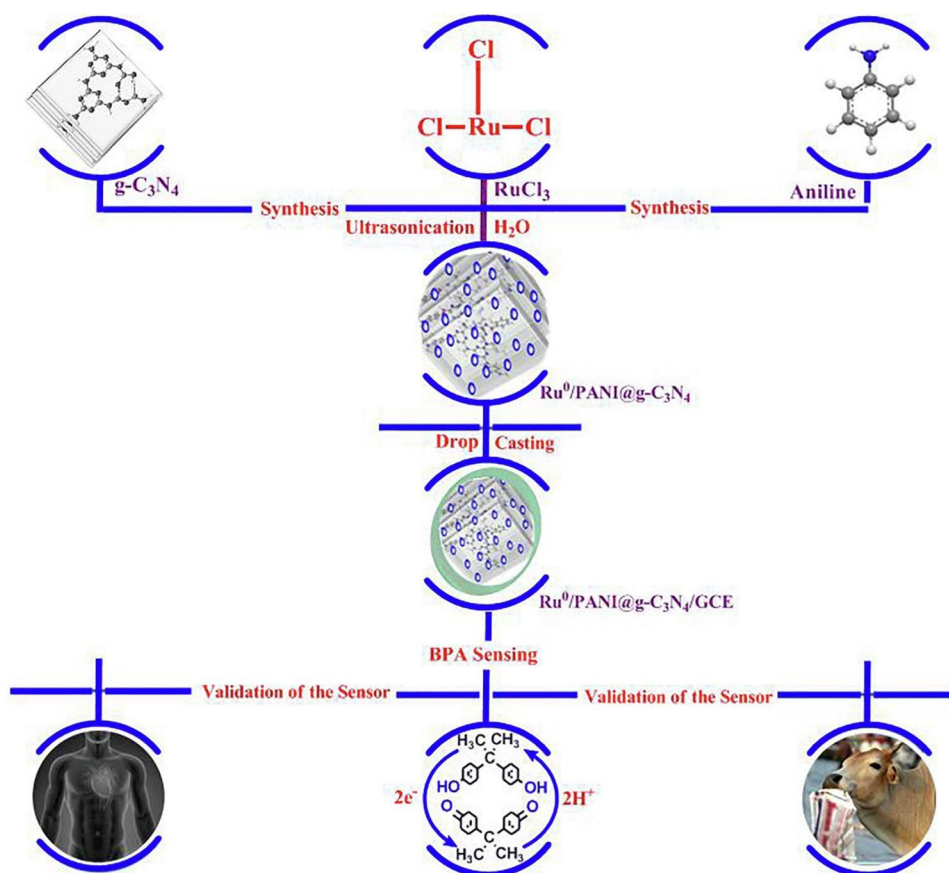
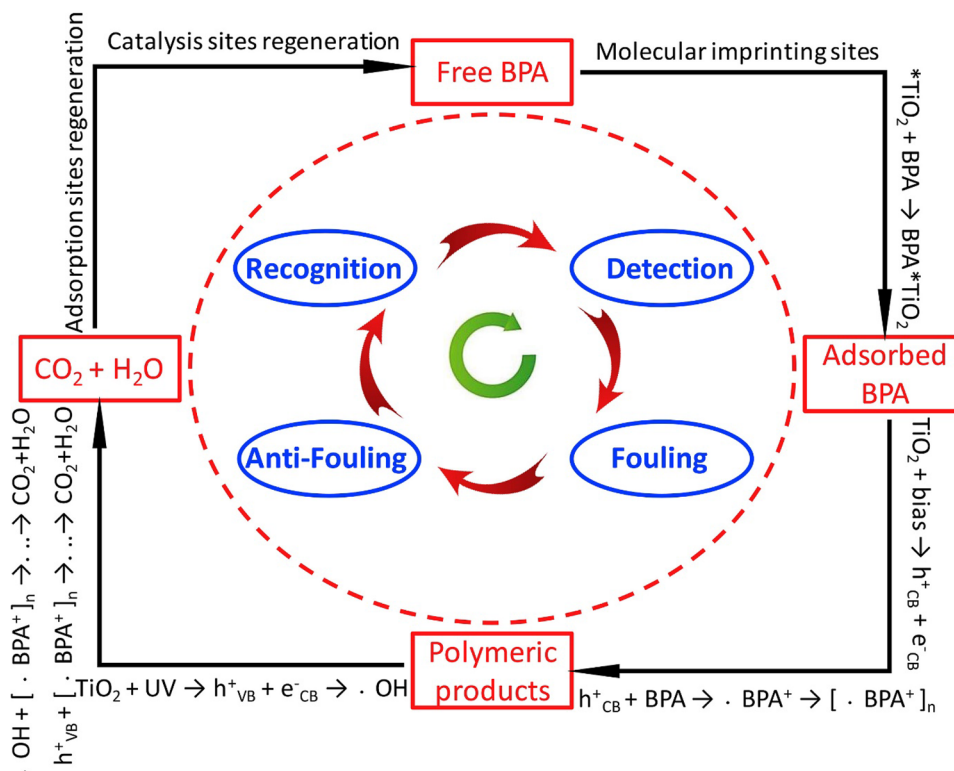


**Fig. 5** The overall reaction that occurred during the detection of HQ on  $\text{TiO}_2$  (reproduced with permission from Copyright Elsevier, Ref. [61])



with Nafion conducting binder was drop dried on a GCE. The sensor detected HQ concentrations ranging from 1.0 to 0.1 nM, with a detection limit of 0.00001053  $\mu\text{M}$  was obtained. The notable features of this platform are the simplicity, ease of use, and low cost.

Similar to this, hydroquinone was quantified using a nanohybrid of  $\text{Co}_3\text{O}_4$  and histidine-functionalised graphene quantum dots (HFGQ) [67]. The nanocomposite assisted in achieving fast energy and promoting electron transfer due to the formation of n/p-heterojunction at the electrode interface. The synergy of  $\text{Co}_3\text{O}_4$  and HFGQ facilitated the oxidation and reduction of hydroquinone on the electrode surface. Hence, a remarkable detection limit of 0.00082  $\mu\text{M}$  was obtained. In our opinion, the detection limit of the sensor obtained in [66] has a low detection limit than the one reported in [67] because Nafion used in the sensor fabrication step makes the platform to be stable. Hence, a significant improvement in the detection limit was obtained.

Another study used  $\text{Co}_3\text{O}_4$  nanoparticles with MWCNTs to simultaneously detect catechol (CC) and hydroquinone (HQ) in seawater [68]. The nanocomposite was prepared via hydrothermal synthesis and used for the fabrication of an electrochemical sensor by a sonicating mixture of MWCNTs@ $\text{Co}_3\text{O}_4$  nanoparticles in 1 mL 0.5% chitosan solution for 300 s. Thereafter, the resulting solution was drop dried on a GCE to form the sensor. The sensor was prepared with, and without the chitosan solution, and the result revealed that the chitosan solution assisted in stabilising the

nanocomposite. Oxidation peaks of 0.176 V and 0.076 V were produced by the electrochemical response of CC and HQ on the constructed sensor (MWCNTs@ $\text{Co}_3\text{O}_4$ /GCE).

$\text{Fe}_3\text{O}_4$  nanoparticles were assembled on the surface of single-walled carbon nanotubes (SWCNTs) for the electrocatalytic oxidation of HQ [69]. Electrostatic interaction between the negatively charged  $\text{Fe}_3\text{O}_4$  nanoparticles and positively charged ammonia-terminated SWCNTs enabled the wet-chemical production of the  $\text{Fe}_3\text{O}_4$  nanoparticles and their decoration with SWCNTs. The nanocomposite ( $\text{Fe}_3\text{O}_4$ @SWCNTs) was dispersed onto the surface of fluorine-doped tin oxide (FTO) to form the sensor. The electrode displayed excellent performance towards the oxidation of HQ. This confirmed the potential application of FTO for sensor fabrication owing to lower cost and not compromising too much on its sensitivity. In our opinion, the uniqueness of this work is the functionalisation of the SWCNTs with positive ammonia-terminated group, which helps attract the negative charge on the surface of the  $\text{Fe}_3\text{O}_4$  nanoparticles. This attraction plays a pivotal role in the stability of the nanocomposite on the FTO surface. When nano-modifiers are dispersed on the surface of FTO, it is important to dry them in the oven at a moderate temperature that will not change the morphology of the material; this concept will assist in stabilising the nanomaterials on the electrode surface.

A highly sensitive and selective electrochemical sensor based on MWCNTs/polydopamine/AuNPs and chitosan was used for the concurrent quantification of HQ

**Table 1** The determination of bisphenol A on different electrochemical platforms

Electrode	Sensor	Detection limit ( $\mu\text{M}$ )	Techniques	References
Paper-based	CB- $\mu$ PAD	0.03	SWV	[37]
SPCE	MagMIP@AuNPs@CBN/SPCE	0.0088	DPV	[38]
PCE	rGO@CNP@GCE	0.001	DPV	[39]
GCE	NiNP/NCN/CS/GCE	0.0045	DPV	[40]
SPCE	Emip/SPCE	0.06	CV	[41]
GCE	MWCNTs@MIPs/GCE	0.02	DPV	[42]
GCE	MIPPy/GQDs/GCE	0.04	DPV	[43]
GCPE	GNPs/IL@GCPE	0.064	DPV	[45]
GCE	PG-BPS@GCE	0.078	DPV	[46]
GCE	MWCNTs@PEI@GCE	0.033	DPV	[47]
GCE	MIPs/AuNPs/GCE	0.011	LSV	[48]
GCE	MWCNTs@AuNPs/GCE	0.004	DPV	[49]
GCE	f-MWCNTs@AuNPs/GCE	0.05	SWV	[50]
GCE	(GNPs/GR)@GCE	0.005	DPV	[51]
GCE	MWCNT-SiO <sub>2</sub> @Au@GCE	0.01	DPV	[52]
PGE	poly (CTAB)@MWCNTs/ PGE	0.005	SWV	[53]
SPCE	MWCNTs@ $\beta$ CD/SPCE	0.01376	LSV	[54]
GCE	Aptamer/NPGF/GCE	0.056	DPV	[55]
GCE	RhB-incubated poly- $\beta$ -CD/EGg/GCE	0.052	DPV	[56]
GCE	AuAgPt-PCD-GO/GCE	0.002	DPV	[57]
GCE	COF, CTpPa-2/GCE	0.02	DPV	[58]
ITO	[Ru(bpy) <sub>3</sub> ] <sup>2+</sup> /ITO	0.0290	LSV	[59]
GCE	RuO/PANI/g-C <sub>3</sub> N <sub>4</sub> @GCE	0.018	DPV	[60]
ITO	MI-TiO <sub>2</sub> /ITO	0.095	DPV	[61]

*MagMIP@AuNPs@CBNS*, magnetic molecularly imprinted polymer@gold nanoparticles@carbon black nanoparticles, *PCE* printed carbon electrode, *eMIPs@SPCE* electrochemical imprinted polymers@screen printed carbon electrode, *MWCNTs@MIPs*, multiwalled carbon nanotubes@molecular imprinted polymer, molecularly imprinted polypyrrole/graphene quantum dots, *GCPE* glassy carbon paste electrode, *MWCNTs@PEI* multiwalled carbon nanotubes@polyethyleneimine, *GNPs/GR* gold nanoparticles dotted graphene, *PGE* pencil graphite electrode,  *$\beta$ CD* beta-cyclodextrin, RhB-incubated poly- $\beta$ -CD/EGg/GCE rhodamine blue poly beta cyclodextrin/electroreduced graphene, *AuAgPt-PCD-GO* AuAgPt ternary alloy nanocrystals (AuAgPt), porous  $\beta$ -cyclodextrin polymer (PCD), and graphene oxide (GO), *COF* CTpPa-2 covalent organic framework, *MI-TiO<sub>2</sub>/ITO* molecularly imprinted titanium (IV) oxide

and CC [70]. Chitosan was used in the fabrication of the sensor owing to its essential analytical features such as good adhesion, film-forming ability, and excellent biocompatibility. The sensor (CS/MWCNTs/PD/AuNPs/GCE) was used to detect HQ and CC in a lake and tap water samples by standard addition method with recoveries of 98.8–103.0% and 98.0–101.5% for CC and HQ, respectively. Similarly, poly(crystal violet) [PCV] was used to modify pencil graphite electrodes (PGE) for the quantification of hydroquinone in the presence of catechol [71]. The crystal violet was electropolymerised on the surface of PGE by cycling a potential from 0.0 to 2.0 V for ten cycles to form PGE@PCV. The measurement of 0.2 mM HQ with bare PGE and PGE@PCV using CV showed a remarkable current enhancement, which is ascribed to the electrocatalytic activity of PCV. The sensor (PGE@PCV) was used for the simultaneous and individual detection

of HQ and CC, with detection limits of 30.35 nM and 27.76 nM. The performance of this sensor was satisfactory and recommendable due to the ease of fabrication of the sensor, the modification route, and the nature of the conducting substrate.

Kumar and his co-workers polymerised murexide on the surface of a glassy carbon electrode for the simultaneous detection of catechol and hydroquinone [72]. The murexide was electrodeposited on GCE by applying potential from  $-0.6$  to  $+1.6$  V at a scan rate of  $0.1 \text{ Vs}^{-1}$ . The poly(murexide) enhanced the electroactive surface area of the bare GCE from  $0.0292$  to  $0.03662 \text{ cm}^2$ . The pH study revealed that the electrocatalytic oxidation of HQ and CC involved the exchange of electrons and protons in the catalytic redox mechanism, and the interference study confirmed that both analytes were oxidised. Figure 6 illustrates the mechanism of murexide electrodeposition on GCE.

Recently, a biomass-derived porous carbon produced from shrimp shells was developed and used to detect hydroquinone [73]. The shrimp shell was utilised to modify glassy carbon electrodes because it contains inorganic calcium carbonate and nitrogen-containing polysaccharides, which are used to make nitrogen-doped porous carbon by pyrolysis. According to the electrochemical characterisation investigations, the shrimp shell porous carbon (SSPC) enhanced the surface area of the bare GCE from 0.0694 to 0.149 cm<sup>2</sup>, indicating that the SSPC has a greater surface area for electrochemical processes. The GCE-SSPC was utilised to detect hydroquinone in lake water samples, yielding impressive results that support the usage of biomass-based carbon for electrochemical applications.

Nitrogen-doped graphene (NGE) was coated with poly(3,4-ethylene dithiophene) PEDOT for the simultaneous detection of CC and HQ [74]. The sensor was constructed by dispersing NGE in dimethylformamide (DMF), and the resulting solution was dried in N<sub>2</sub> to form NGE/GCE. Thereafter, PEDOT was electrodeposited on NGE/GCE using a solution containing 0.1 M lithium perchlorate and 0.01 M EDOT to form NGE/GCE@PEDOT. According to the electrochemical impedance spectroscopy results reported by the authors, the NGE/GCE demonstrated a small quasi-semicircle at high frequency and a straight line at low frequency, indicating quick electron transfer kinetics. At the same time, the Nyquist plot

of NGE/GCE@PEDOT is a linear curve at all frequencies. This result confirmed that the electron transfer process is diffusion controlled and exhibits excellent electron conductivity. Finally, the sensor was used for the detection of HQ and CC in lake water by spiking with different concentrations (1.5 and 10 μM). The PEDOT prevented the leaching of the NGE in the analyte solution and assisted in the peak separation of the analytes during detection.

Porphyrin-functionalised AuNPs and graphene worked together to produce an amazing light-on-off photoelectrochemical (PEC) sensor for HQ [75]. The sensor was prepared by wiring AuNPs into the matrix of graphene sheets using sodium borohydride as the reducing agent. Thereafter, sulfhydryl porphyrin was assembled on the AuNPs/graphene sheets by Au–S bond. The composite was used in modifying indium tin oxide (ITO) and the sensor showed intriguing photoelectrochemical behaviour towards the oxidation of hydroquinone at 0 V under white light illumination. The graphene sheets served as the transporter and acceptor of the photogenerated electrons in the porphyrin/AuNPs film, which reduced the charge transfer resistance and enhanced the PEC performance. Porphyrin was utilised as a light harvester, and the AuNPs enhanced the electron transport by collecting and transferring the photoexcited electrons. A larger photocurrent signal was attained at the porphyrin/AuNPs/graphene film, and it detected HQ to a

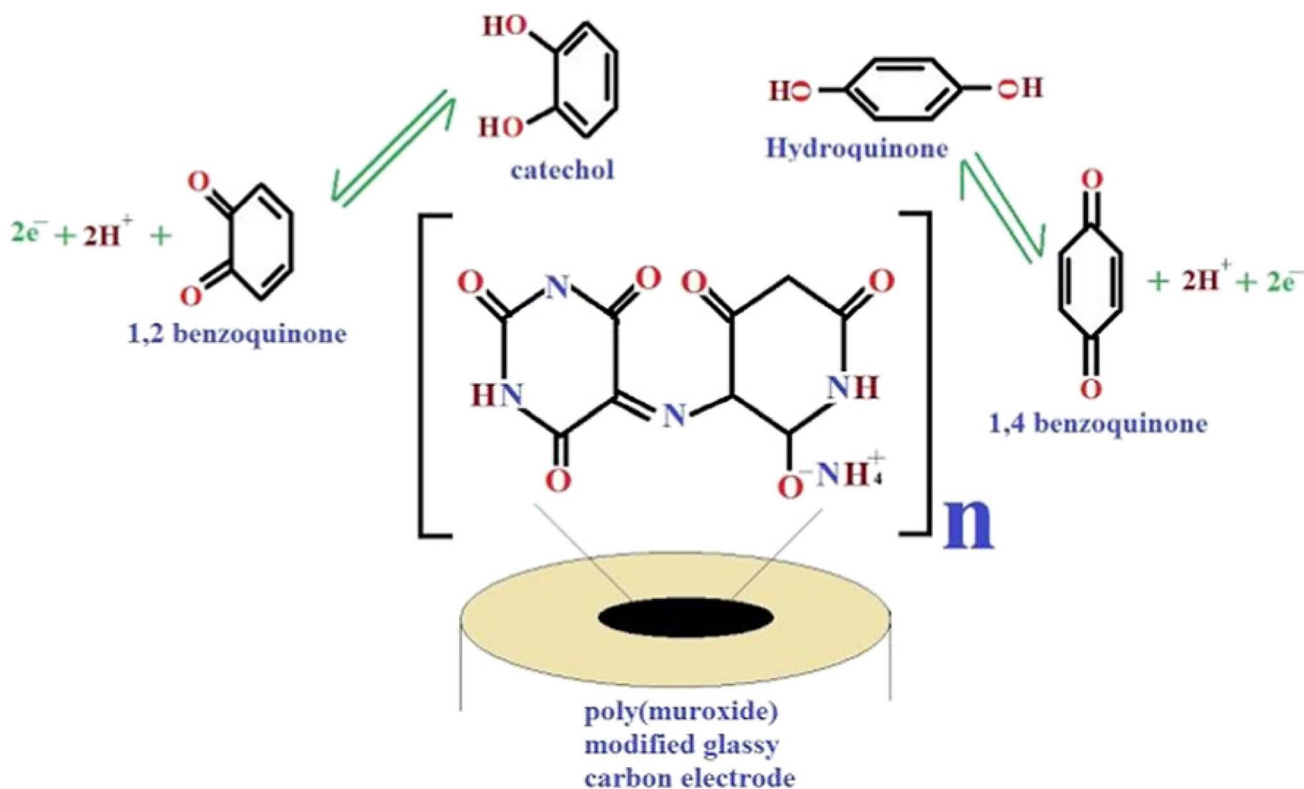


**Fig. 6** The proposed electropolymerisation mechanism of murexide on a GCE (reproduced with permission from Ref. [72])

concentration limit down to 4.6 nM. The sensor fabrication scheme is depicted in Fig. 7. It is recommended that future studies should employ ascorbic acid for the reduction of graphene in place of  $\text{NaBH}_4$ , which is toxic and environmentally unfriendly or better still use electrochemical reduction method.

For the electrochemical determination of HQ, Chen et al. prepared copper oxide on histidine-functionalised graphene quantum dots (His-GQDTs) [76]. The nanocomposite was formed by reacting  $\text{Cu}^{2+}$  ions with His-GQDTs via a coordination reaction; the product formed was oxidised in air to form a CuO-His-GQDTs hybrid. The nanocomposite's open-porous structure and three-dimensional architecture were both visible in the SEM/TEM images. The author alluded that the nanocomposite morphology assisted in the amplification of the detection signal for the electrochemical determination of HQ. The open-porous structure of the nanomaterial aided the entrapment of the analyte on the detection platform. Hence, a remarkable detection limit of 0.00031  $\mu\text{M}$  was obtained.

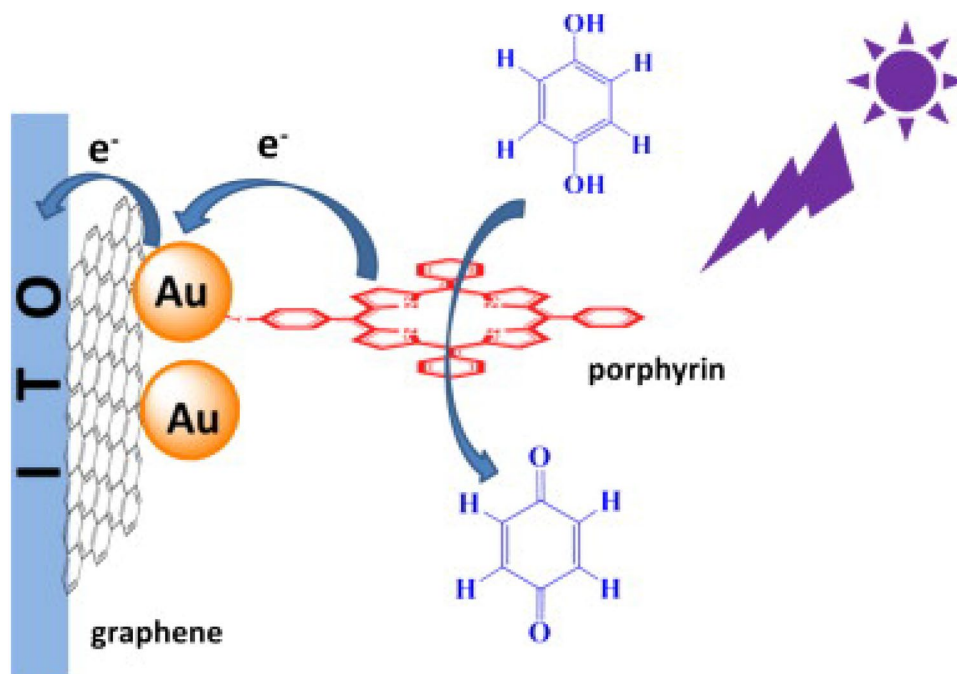
A water-soluble zinc meso-tetra (4-carboxylicphenyl) porphyrin (ZnTCPP) was assembled on rGO/AuNPs/Cs by  $\pi$ - $\pi$  nanoassembly strategy to form rGO/AuNPs/Cs@ZnTCPP, which was employed in the construction of HQ sensor [77]. The nanocomposite was eco-friendly and dispersed uniformly on the ITO electrode for the PEC detection of hydroquinone. The photoanode displayed a good photocurrent response at  $-0.2$  V under xenon lamp illumination; this is due to the excellent conductivity of AuNPs, fast electron transfer ability of rGO, and the synergistic effect of the nanocomposites. When HQ was immobilised on the sensor

(rGO/AuNPs/Cs@ZnTCPP/ITO), it acted as the hole scavenger by providing electrons to the metalloporphyrin molecule and aided in reducing the recombination of the electron-hole pair. Thus, the enhancement in the photocurrent response was due to the oxidation of HQ to benzoquinone (BQ), which enhanced the efficiency of the charge separation. It is important to note that the nanomaterials employed for photoelectrochemical detection of analyte must be photoactive or blended with photoactive materials.

A ternary composite material (polyaniline@ $\text{Fe}_2\text{O}_3$ @rGO) was synthesised, characterised, and applied for the detection of HQ [78]. The  $\text{Fe}_2\text{O}_3$ @rGO was prepared by hydrothermal synthesis and the PANI was incorporated into the matrix of  $\text{Fe}_2\text{O}_3$ @rGO by in situ polymerisation. The sensor was developed by drop drying 10  $\mu\text{L}$  aliquot of 0.5  $\text{mg mL}^{-1}$  polyaniline@ $\text{Fe}_2\text{O}_3$ @rGO onto the surface of GCE and allow to dry at ambient temperature. The sensor displayed excellent electrocatalytic activity for hydroquinone oxidation. The oxidation current of hydroquinone is linear within the concentration range of  $1 \times 10^{-7}$ – $5.5 \times 10^{-4}$  M, and a detection limit of  $6 \times 10^{-8}$  M was reported. It is important to highlight that the author employed PANI to shield and prevent  $\text{Fe}_2\text{O}_3$ @rGO from leaching into the analyte solution. Proof-of-concept studies must be carried out when more than one modifier is used; this will help provide information on the contribution of each modifier during sensor development.

Eco-friendly prepared reduced graphene oxide (rGO) was decorated on marigold-like ZnO nanocomposite for the determination of HQ [79]. The rGO was prepared by sonicating graphite oxide for 2 h, followed by the addition of ammonia and ascorbic acid, which was used to deoxidise

**Fig. 7** Schematic view of the PEC fabrication and the oxidation of HQ on ITO electrode (reproduced with permission from Copyright Elsevier, Ref. [75])



the GO. Thereafter, the resulting solution was stirred, centrifuged, washed with deionised water, and dried in an oven for 12 h. The ZnO was decorated on reduced graphene oxide by electrochemical co-preparation and sonochemical method to form rGO@ZnO. The scheme for the synthesis is displayed in Fig. 8. The electroactive surface area of the rGO@ZnO/GCE is 2.2 times more than the bare GCE, confirming the superiority of the electrocatalytic material over the bare GCE. The DPV technique was used in this study because of its sensitivity and ability to remove non-faradaic current resulting in an efficient analytical signal, the detection limit, and sensitivity of  $0.01 \mu\text{M}$  and  $8.08 \mu\text{A}\mu\text{M}^{-1} \text{cm}^{-2}$  were obtained. For future studies, ascorbic acid should be employed as an environmentally friendly reducing agent in place of pungent and toxic ammonia solutions commonly used for the synthesis of nanomaterials.

Metal–organic framework (MOF) and reduced graphene oxide were used to modify a carbon paste electrode (CPE) for the quantification of CC and HQ [80]. The composite was prepared by one-pot hydrothermal synthesis, and graphene oxide was partially reduced at the same time. The sensor was prepared by adding rGO@MOF and graphite powder (weigh ratio 14:1), followed by thorough mixing with paraffin to form a paste, which is carefully placed inside a CPE to form the sensor (rGO@MOF/CPE). The platform was used in the quantification of both analytes in lake water samples, and the result obtained from DPV showed small

deviations from the standard ( $<3\%$ ), which was far better than the results obtained from high-performance liquid chromatography (HPLC). Based on our current understanding, the primary drawback associated with utilizing a carbon paste electrode on this platform is the potential for inconsistent results emanating from human error.

Graphene oxide and 3,4-ethylene dioxathiophene (EDOT) were co-polymerised on a glassy carbon electrode for the simultaneous detection of CC and HQ [81]. The sensor was fabricated by dispersing a mixture of GO (1 mg/L) and EDOT (0.01 M) in 5 mL deionised water and ultrasonicated for half an hour. The resulting solution was electrodeposited on a GCE by cycling potential from  $-0.2$  and  $1.2 \text{ V}$ , at a scan rate of  $100 \text{ mVs}^{-1}$ , under magnetic stirring and nitrogen bubbling. The successful electrodeposition of GO@EDOT on the electrode surface was demonstrated by the formation of a bright blue layer with a metallic sheet on the GCE surface. The poly(EDOT) revealed considerable roughness and a loose structure made up of wrinkled paper-like sheets, from the scanning electron microscopy (SEM) and transmission electron microscopy reported by the authors. The morphology of the nanocomposite assisted in promoting the diffusion of the analytes from the electrolyte to the electrode surface. Hence, the sensor was able to simultaneously detect CC and HQ down to  $1.6 \mu\text{M}$  for both analytes. The stability of the sensor was interrogated by performing 50 consecutive potential scans of a

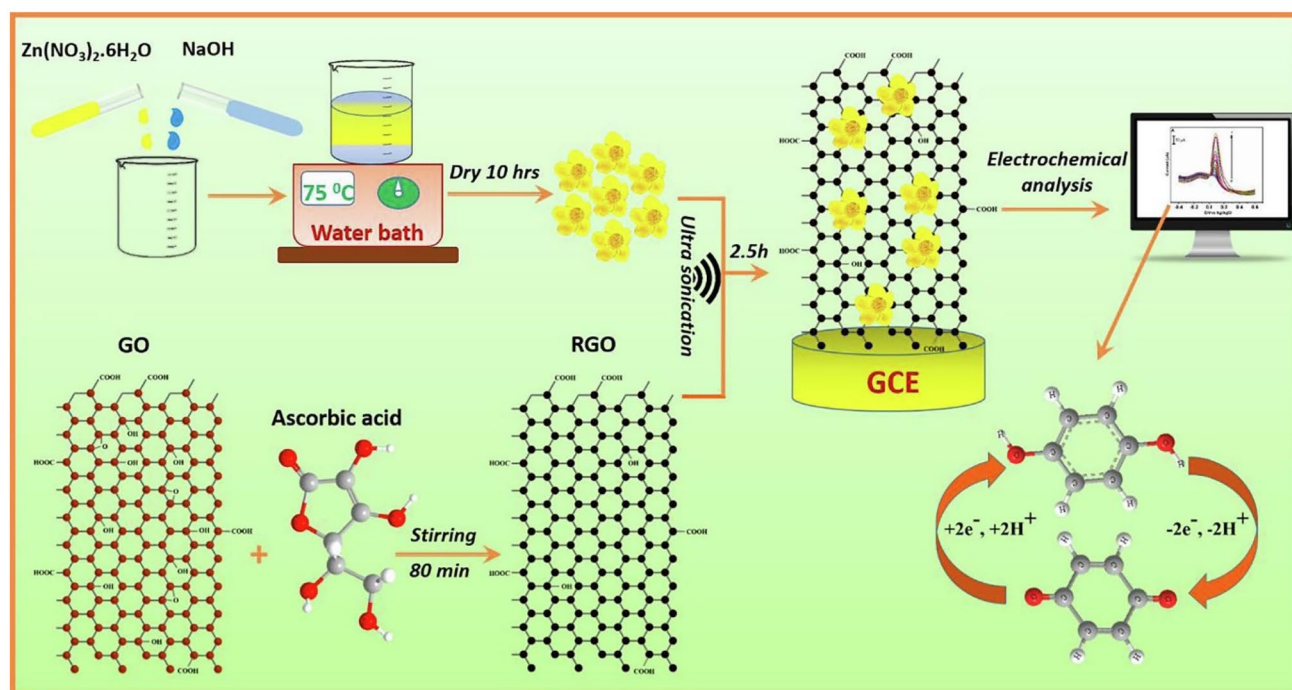


**Fig. 8** Graphical display of the synthesis and detection of HQ using rGO@ZnO/GCE (reproduced with permission from Copyright Elsevier, Ref. [79])

solution containing the same concentrations of CC and HQ (0.1 mM) prepared in 0.1 M PBS. There was a 5.9% and 6.5% reduction in the peak current signals of HQ and CT. The novelty of this sensor based on our judgement is associated with the co-electrodeposition of both modifiers on the glassy carbon electrode; this invariably helped in boosting the sensor sensitivity, stability, and reproducibility. Peak current signals of HQ and CT were reduced by 5.9% and 6.5%, respectively. The co-electrodeposition of both modifiers on the glassy carbon electrode is what gives this sensor its originality. This always helps to increase the sensor's sensitivity, stability, and reproducibility.

Octadecylamine-functionalised graphene vesicles (OA-GV) were used as the immobilisation layer on a glassy carbon electrode for the voltammetric sensing of HQ [82]. The introduction of octadecyl amine into the matrix of graphene oxide assisted in increasing its surface area ( $1853.2 \text{ m}^2\text{g}^{-1}$ ) and promoting the synergy in the electrochemistry between OA-GV and HQ. The sensor was fabricated by dispersing 10 mg OA-GV in distilled water, and the resulting solution was mixed with 1% chitosan solution. The final solution was dropped dried on the GCE surface to form the sensor. The constructed sensor was used in the determination of HQ in diluted wastewater, skin toner, and lake water samples.

Hydroquinone (HQ) and resorcinol (RS) were quantified using an electrodeposited green and controlled graphene-gold nanocomposite layer on a GCE [83]. The GO was electrochemically reduced and deposited on the surface of GCE by applying a  $-1.2 \text{ V}$  potential for 50 s at  $10 \text{ }^\circ\text{C}$  to generate GCE@GO. The GO was electrochemically reduced and dispersed in water for a few minutes to form homogenous GO dispersion. Following that, GCE@GO/AuNPs were prepared by electrochemically depositing gold nanoparticles onto the surface of GCE@GO at a constant potential of  $-0.25 \text{ V}$  for 50 s in a solution of  $0.01 \text{ mmol l}^{-1}$  chloroauric acid produced in  $0.5 \text{ mol l}^{-1} \text{ H}_2\text{SO}_4$ . With a sensitivity of  $30.5 \text{ A M}$ , the sensor displayed high electrocatalytic activity towards both analytes, with a sensitivity of  $30.5 \text{ } \mu\text{A } \mu\text{M}^{-1} \text{ cm}^{-2}$  and  $117.83 \text{ } \mu\text{A } \mu\text{M}^{-1} \text{ cm}^{-2}$  for HQ and RS, respectively. The beauty of this platform is based on the modification route used in the fabrication of the sensor, and both modifiers were anchored on GCE by electrochemical modification routes, which is more suitable than drop drying and drop coating.

Au@Pd core-shell nanocomposites were produced using a chemical reduction technique and used to modify a GCE to determine hydroquinone [84]. By adjusting the amount of the precursor, different ratios of Au@Pd core-shell nanocomposites were optimised, but the ( $n_{\text{Au}}:n_{\text{Pd}} = 3.6$ ) electrochemical signature produced the best electrochemical signature that was employed to modify the GCE. The oxidation of HQ at a peak potential of  $0 \text{ V}$  and a potential window of  $-0.3$  to  $0.3 \text{ V}$  caused the sensor to become extremely responsive and sensitive. A chemical reduction method was used in the

synthesis of Au@Pd core-shell nanocomposites, which was employed in the modification of a GCE for the determination of hydroquinone [84]. Different ratios of Au@Pd core-shell nanocomposites were prepared by tuning the amount of precursor, but the best electrochemical signature was derived from the ( $n_{\text{Au}}:n_{\text{Pd}} = 3.6$ ) and used to modify the GCE. The sensor was very sensitive and responsive towards the oxidation of HQ at an oxidation peak of  $0 \text{ V}$  and a potential window of  $-0.3$  to  $0.3 \text{ V}$ .

AuNPs@rGO@WO<sub>3</sub> was prepared using a one-pot polyol and metal-organic decomposition (MOD) approach, which was used for the simultaneous detection of hydroquinone and catechol [85]. To synthesise the nanocomposite, graphene oxide was added to a mixture of (glycerol, H<sub>2</sub>WO<sub>4</sub>, and HAuCl<sub>4</sub>). The resulting mixture was heated for 60 min at  $190 \text{ }^\circ\text{C}$  while being vigorously magnetically stirred. As the colour of the suspension changed at this temperature from yellow to pale green to deep blue suspension (DBS), it was reported that WO<sub>3</sub>NPs had been produced and that Au<sup>3+</sup> and GO had been immediately reduced in the glycerol. The DBS was then dried for 120 min at  $170 \text{ }^\circ\text{C}$ . The dried sample was then calcined at  $500 \text{ }^\circ\text{C}$  for 4 h to create the AuNPs@rGO@WO<sub>3</sub> nanocomposite. The sensor was developed by dropping a nanocomposite suspension onto a GCE and drying it there for 60 min at  $60 \text{ }^\circ\text{C}$ . The author reported that the AuNPs improved the conductivity and electrocatalytic activity of the sensor, and rGO created a rich electroactive and binding site. With a recovery rate of 83–119%, the sensor was successfully used in the simultaneous detection of analytes in diverse water samples.

By using acid etching and an alkaline intercalation process, titanium carbide (Ti<sub>3</sub>C<sub>2</sub>) was adorned with a metal-organic frame-nitrogen doped porous carbon (MOF-NPC) for the determination of hydroquinone [86]. The MOF-NPC prevents the Ti<sub>3</sub>C<sub>2</sub> sheets from restacking and enables the sensing of HQ via hydrogen-bond interaction. The nanocomposite contains surplus  $-\text{OH}$  and  $\text{C}-\text{N}$  functional groups from the alkaline-Ti<sub>3</sub>C<sub>2</sub> and NPC. These functional groups help in the determination of HQ on the premise of benzenediol/benzoquinone redox reactions. The sensor was reported to possess excellent electrical conductivity and detected HQ down to  $4.8 \text{ nM}$  with a wide linear range of  $0.5$  to  $150 \text{ } \mu\text{M}$ .

Similarly, two-dimensional (2-D) hierarchical Ti<sub>3</sub>C<sub>2</sub> nanosheets were incorporated into the matrix of MWCNTs in the development of a smart sensor for the concurrent detection of HQ and CC [87]. The nanocomposite was created by ultrasonically combining 2-D hierarchical Ti<sub>3</sub>C<sub>2</sub> with MWCNTs. The sensor possesses excellent biocompatibility, a large specific area, superior metallic conductivity, and unique electronic conductivity. These analytical features assisted the sensor in improving the electrocatalytic oxidation of both analytes in industrial wastewater samples using the standard addition method.

An efficient and cost-effective NaOH nanorod was used for the simultaneous detection of HQ, CC, and RC [88]. The sensor was prepared by electrodeposition of a 3 M NaOH solution on a GCE for 20 s at a current of 0.2 mA. Several parameters, including the effect of deposition time, deposition current, and the concentration of NaOH, were optimised for the preparation of NaOH nanorod. The SEM images confirmed the uniform distributions of the NaOH

nanorod film on the GCE surface. It is noteworthy that there was a prominent peak separation in the signal of the dihydroxybenzene isomers (Fig. 9). The sensor was able to detect all the analytes to detection limits of 0.01, 0.01, and 0.09 for HQ, CC, and RC, respectively. In our view, this sensor is arguably the cheapest and easiest to design because it does not involve the use of complex and toxic chemicals. However, the author failed to discuss the

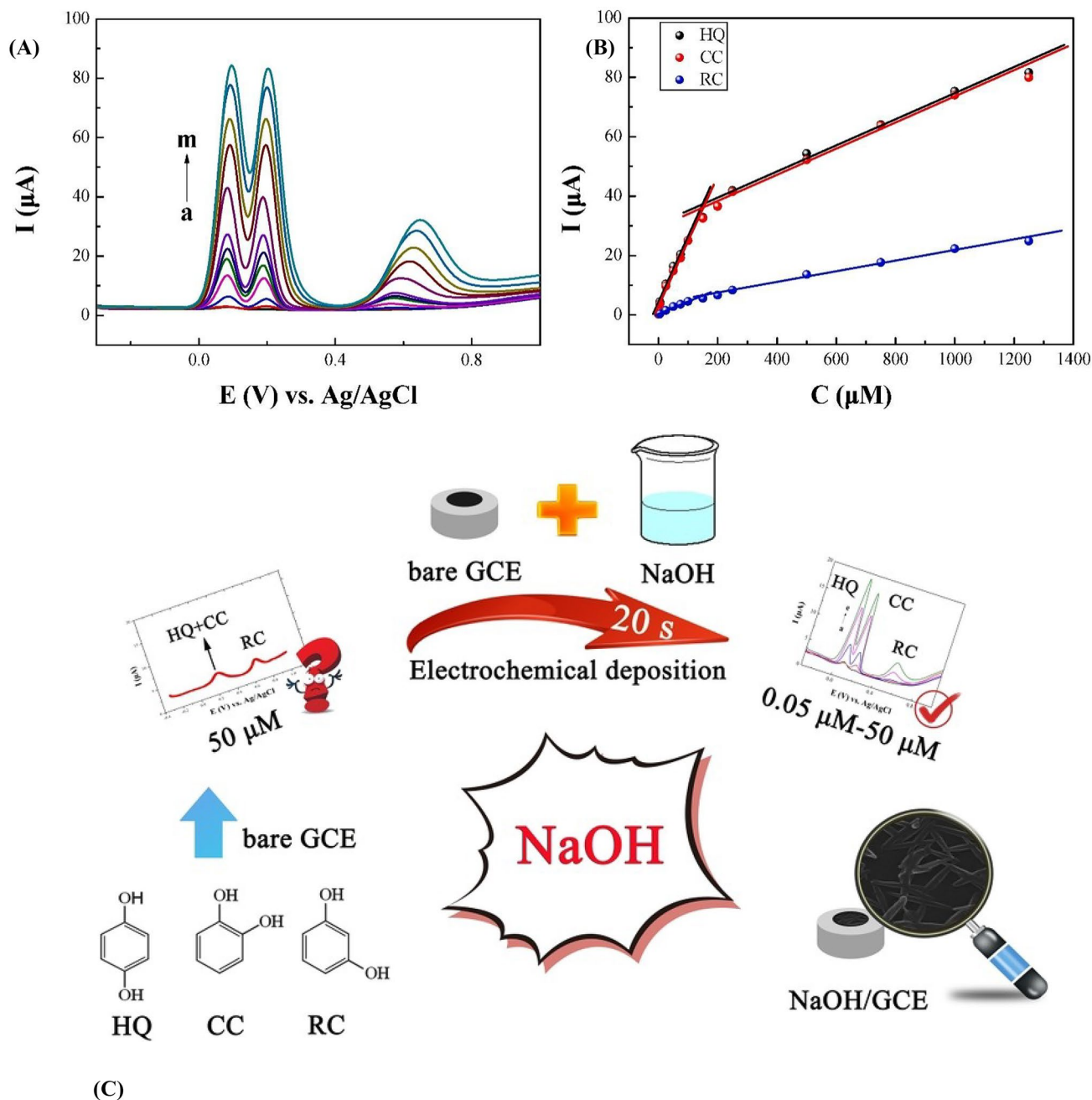


**Fig. 9** **A** The simultaneous detection of HQ, CC and RC using GCE-NaOH nanorod. **B** The calibration graph of the simultaneous detection of HQ, CC, and RC. **C** Scheme for the detection of the analytes

using NaOH nanorod (reproduced with permission from Copyright Elsevier Ref. [88])

stability of the NaOH nanorod on the electrode surface because of the solubility of NaOH.

A printex 6L carbon nanoball (CNB) was purchased from Degussa Germany and used to modify GCE for the simultaneous detection of hydroquinone and paracetamol (PCM) [89]. The SEM image revealed that the nanoballs are not perfectly spherical, but they form an ultrathin and porous film on the surface of the GCE. The electrochemical impedance spectroscopy was used to evaluate the heterogeneous electron rate constant ( $K_{app}$ ) and the charge transfer resistance ( $R_{ct}$ ) of the bare GCE and the modified electrode. The  $K_p$  values of 4.76 and 3.22 were obtained for GCE and GCE/CNB, while the  $R_{ct}$  of the GCE decreased from 107.33 to 72.63  $\Omega$ . The  $K_{app}$  and  $R_{ct}$  values of the CNB confirmed the conducting nature, which facilitated electron transfer on the electrode surface. The limits of detection of HQ and PCM were 8.0 and  $82.0 \times 10^{-9}$  molL<sup>-1</sup>, respectively. The low detection limits obtained for these analytes are attributed to the presence of the hydroxyl and carboxylic functional groups present on the surface of CNB. In our opinion, the author should have synthesised a carbon nanoball in the laboratory and compared the result obtained with the one obtained commercially from Degussa, Germany.

A bare SPCE was used for the ultrasensitive detection of hydroquinone, paracetamol, and estradiol in tap water [90]. Before using the SPCE for electrochemical analysis, it was pre-treated with 0.5 M sulphuric acid using CV in a potential range from -2.5 to 2.5 V. The SEM image and the energy-dispersive X-ray (EDX) revealed that the pre-treatment did not affect the morphology of the electrode but removed the non-conducting residues from the printing ink. The SPCE was used in the determination of the analytes and was not affected by common interference ions. The detection limits obtained for the analytes were comparable to those obtained using HPLC and gold-standard methods. The beauty of this research, in our opinion, was that this platform was employed for the detection of the analytes without the use of any nanomaterials; this helps to reduce the sensor cost, and it is impressive that a bare SPCE was able to detect the analytes simultaneously. The sensor's sensitivity is low because the author did not employ nanomaterials for the sensor fabrication; this confirms the gap of not employing smart nanomaterials for sensor development.

Deng et al. synthesised a zirconium-based mesoporous organic framework (MOF) on a mesoporous carbon (MC) for the simultaneous quantification of hydroquinone, catechol, and resorcinol [91]. The amount of MC, scan rate studies, and pH were all investigated as optimisation criteria. The electrochemical oxidation of the analytes depends on the solution acidity because the proton plays a substantial role in the electrode reaction. The pH study was investigated using DPV in a pH range from 4.0 to 9.0. The results showed that the oxidation peaks of the analyte increase

with increasing pH value from 4 to 6, and the oxidation peaks decrease after this pH. Thus, pH 6 was used for the electrochemical detection of the analytes, with detection limits of 0.056  $\mu$ M, 0.072  $\mu$ M, and 3.51  $\mu$ M for HQ, CT, and RS, respectively. The author fails to give details why higher and lower pH values were not explored for the optimisation process. Researchers should investigate all pH ranges to have an experimental grasp of the impact of pH on sensor sensitivity. Tables 2 and 3 gives a summary report of various types of sensors used for the determination of HQ in water.

Summarily, various smart nanomaterials have aided the detection of hydroquinone as well as the simultaneous detection of organic pollutants. The detection of one of the notorious organic pollutants is discussed in the next section.

### Electrochemical Determination of Nitrophenol (NPhs)

Nitrophenols (NPhs), which include m-nitrophenol, p-nitrophenol, and o-nitrophenol, are widely utilised in the production of medications, insecticides, and colours [92, 93]. The toxicity and stability of NPhs are responsible for their adverse effects on plants, animals, and humans [92]. Nitrophenol exposure, whether from ingesting or inhalation, can result in sleepiness, nausea, cyanosis, and headaches [92, 93]. Nitrophenol detoxification is difficult due to its high chemical stability and resistance to microbial breakdown [94, 95]. Because of their toxicity, anthropogenic, inhibitory, and bio-refractory qualities, nitrophenols have been identified as infamous pollutants by the USEPA [96]. In addition, the allowable limit of 4-NPhs in drinking water has been set at 0.43  $\mu$ M. Hence, nitrophenol measurement is critical for environmental protection.

Wiench et al. prepared reduced graphene oxide (rGO) for the electrochemical measurement of 4-nitrophenol [97]. Hummer's method was used to prepare graphene oxide, which was then hydrothermally reduced at three distinct temperatures (120 °C, 150 °C, and 180 °C) to form reduced graphene oxide. The sensor was made by dispersing 4 mg of rGO in 1 mL DMF and ultrasonically dissolving it for 3 h to obtain a homogeneous solution (HS). The surface of the GCE was modified with 2.5  $\mu$ L HS to produce rGO/GCE. The GCE's charge transfer resistance was lowered from 348 to 150  $\Omega$ , indicating that rGO facilitates electron transfer on the electrode surface. As a result, it was utilised to quantify 4-nitrophenol with a detection limit of 42  $\mu$ M. However, the hydrothermal approach was utilised to reduce graphene oxide to rGO, which is environmentally friendly from our perspective. However, for future studies, researchers should employ the electrochemical reduction method to save power, which invariably lowers the sensor's cost.

**Table 2** Various types of materials used to fabricate sensors for the quantification of HQ in water

Sensor	Linear range ( $\mu\text{M}$ )	LOD ( $\mu\text{M}$ )	Techniques	References
$\text{Co}_3\text{O}_4$ @GCE	0.0001–0.1	0.00001053	SWV	[66]
$\text{Co}_3\text{O}_4$ -His-GQD@GCE	0.00002–0.8	0.00082	DPV	[67]
$\text{Co}_3\text{O}_4$ /MWCNTs@GCE	10–800	5.6	DPV	[68]
$\text{Fe}_2\text{O}_3$ /CNTs@FTO	1–80	0.5	DPV	[69]
MWCNTs@PDA@AuNPs@GCE	0.1–10	0.035	DPV	[70]
PCV@MPGE	10.37–109.1	0.03035	DPV	[71]
Poly(murexide)@GCE	0.1–0.8	0.23	CV	[72]
PEDOT/NGE@GCE	1–10	0.26	DPV	[74]
Porphyrin/AuNPs/graphene@ITO	0.02–0.24	0.0046	PCE	[75]
CuO-His-GQD@GCE	0.001–40	0.00031	DPV	[76]
rGO/AuNPs/CS/ZnTCPP@GCE	0.005–0.3	0.0005	PCE	[77]
Polyaniline- $\text{Fe}_2\text{O}_3$ -rGO@GCE	0.1–550	0.0006	DPV	[78]
RGO@ZnO@GCE	0.1–92	0.01	DPV	[79]
RGO/MOF@CPE	4–1000	0.66	DPV	[80]
PEDOT@GO@GCE	2.5–200	1.6	DPV	[81]
OA-GV@GCE	0.01–1.0	0.0049	DPV	[82]
Graphene-AuNPs@GCE	0.16–1.2	0.0052	DPV	[83]
Au@Pd@GCE	4–5000	0.63	DPV	[84]
AuNPs/RGO/ $\text{WO}_3$ @GCE	0.1–10	0.036	DPV	[85]
Alk- $\text{Ti}_3\text{C}_2\text{N}$ -PC@GCE	0.5–150	0.0048	DPV	[86]
$\text{Ti}_3\text{C}_2$ /MWCNTs@GCE	2–150	0.0066	DPV	[87]
NaOH nanorods@GCE	0.03–1500	0.01	SWV	[88]
CNB@GCE	0.08–2.3	0.0013	DPV	[89]
Pre-treated-SPCE	0.5–10	0.185	DPV	[90]
UiO-66/MC@GCE	0.5–100	0.056	DPV	[91]

By modifying GCE with cyclodextrin (CD) and chitosan-functionalised rGO composite film, a new electrochemical sensor for simultaneous detection of ortho- and para-nitrophenols was developed [98]. The electrostatic attraction provided by host–guest recognition sites on CD and avalanche functional groups on chitosan molecules aided the adsorption of nitrophenol on the electrode surface. The nitroaromatic/hydroxylamine redox reactions were used to detect ortho- and para-nitrophenols simultaneously. The detection limits of both isomers were 0.018  $\mu\text{M}$  and 0.016  $\mu\text{M}$ , respectively, which were significantly lower than the detection limits reported by Wiench et al.; the explanation for this notable difference was attributed to the nanocomposite's synergistic effects as well as the chitosan's ability to operate as an efficient mediator to enhance nitrophenol migration on the electrode surface.

Controlled synthesis of rGO-supported AgNPs was used for the determination of 4-nitrophenol (4-NP) [99]. The nanocomposite was prepared by optimisation of various reaction times (2 h, 6 h, 10 h, and 15 h) in Tollens' reagent. The morphological studies revealed that the reaction time at 15 h gave a complete spherical AgNPs with an average particle size of 16 nm. Hence, it was used for the electrochemical reduction of 4-NP with a higher Faradaic current at an overpotential of  $-0.5$  V.

The platform was selective and stable in the presence of different organic compounds including 2-aminophenol (2-AP), 3-aminophenol (3-AP), 4-aminophenol (4-AP), 2, nitrophenol (2-NP), and 2,4-dichlorophenol (2,4-DCP). The scheme for the detection of 4-NP using rGO@AgNPs is displayed in Fig. 10.

Ultra-stable perfluorinated sulfonic acid (PFSA)-Ag colloid was prepared and used for the quantification of 4-nitrophenol [100]. The PFSA-Ag colloid was synthesised by dispersing PFSA in a mixture of ( $\text{H}_2\text{O}$  and isopropanol) at 200 °C for 4 h. Thereafter,  $\text{AgNO}_3$  was added into the resulting solution and transferred into a sealed hydrothermal kettle for 4 h in a rotating oven. Because of the strong attraction between the PFSA sulfonated groups and Ag ions, the PFSA prevented the agglomeration of AgNPs during nucleation. The PFSA-Ag nanocomposite was coated on the carbon paper electrode and used for the quantification of 4-NP. The mechanism of the sensing process involves the reduction of 4-NP to 4-hydroxy aminophenol (4-HP) and the oxidation of 4-HP to 4-nitrosophenol, followed by a subsequent reversible reduction. It is worth noting that the PFSA-Ag colloid demonstrated remarkable stability after 60 days of storage with no precipitation marks.

**Table 3** The report on various sensors for the electrochemical detection of nitrophenol A in water

Sensor	Linear range ( $\mu\text{M}$ )	Detection limit ( $\mu\text{M}$ )	Techniques	References
rGO@GCE	50 to 800	42	DPV	[97]
RGO-CD-CS@GCE	5–40	0.016	DPV	[98]
RGO@AgNPs	0.01–0.1	0.0012	SWV	[99]
PFSA-AgNPs@GCE	0.02–10	0.015	DPV	[100]
TA@Fe <sub>3</sub> O <sub>4</sub> -AgNPs/GCE	0.1–68	0.033	DPV	[101]
AgAP-bPGE	10–100	1.1	DPV	[102]
AgPd@UiO-66-NH <sub>2</sub> /GCE	100–370	32	DPV	[103]
AgNWs-PANI/GCE	0.6–32	0.052	DPV	[104]
PANI-GITN-GCE	0.01–4	0.0024	DPV	[105]
PANI/GO@GCE	0.6–0.14	0.2	CV	[106]
PDDA-G@GCE	0.06 to 110	0.02	LSV	[107]
PEDOT: PSS/ITO	0–80	0.12	DPV	[108]
Thiophene-GCE	0.3–15	0.05	DPV	[109]
FeOx/TiO <sub>2</sub> @mC@GCE	5–310	0.183	Amperometry	[110]
(Fe <sub>3</sub> O <sub>4</sub> -Pt) NPs-GCE	0.1–1.5	0.0337	DPV	[111]
Fe <sub>3</sub> O <sub>4</sub> @AT-COF/GCE	0.005–4.0	0.5925	DPV	[112]
NPG-GCE	0.25–10	0.1	CV	[113]
C/N-AuNPs@GCE	0.1–32	0.072	DPV	[114]
Au-CuNPs@GCE	0.04–4.5	0.006	SWV	[115]
Au/CaCO <sub>3</sub> @GCE	0.1–100	0.0054	CV	[116]
CeO <sub>2</sub> -Cu <sub>2</sub> O@GCE	74–375	2.03	CV	[117]
CH/CeO <sub>2</sub> -Co <sub>2</sub> O <sub>3</sub> @GCE	11.80 to 48.75	0.46	CV	[118]
ZnCo <sub>2</sub> O <sub>4</sub> @GCE	1–4000	0.3	DPV	[119]
ZnO NPs@fMWCNTs/SPCE	0.06–100	0.0 13	DPV	[120]
$\alpha$ -MnO <sub>2</sub> /MWCNTs@GCE	30–475	0.644	Amperometry	[121]

CH/CeO<sub>2</sub>-Co<sub>2</sub>O<sub>3</sub>@GCE chitosan/cerium oxide@cobalt oxide@glassy carbon electrode, C/N-AuNPs@GCE nitrogen doped gold nanoparticles glassy carbon electrode

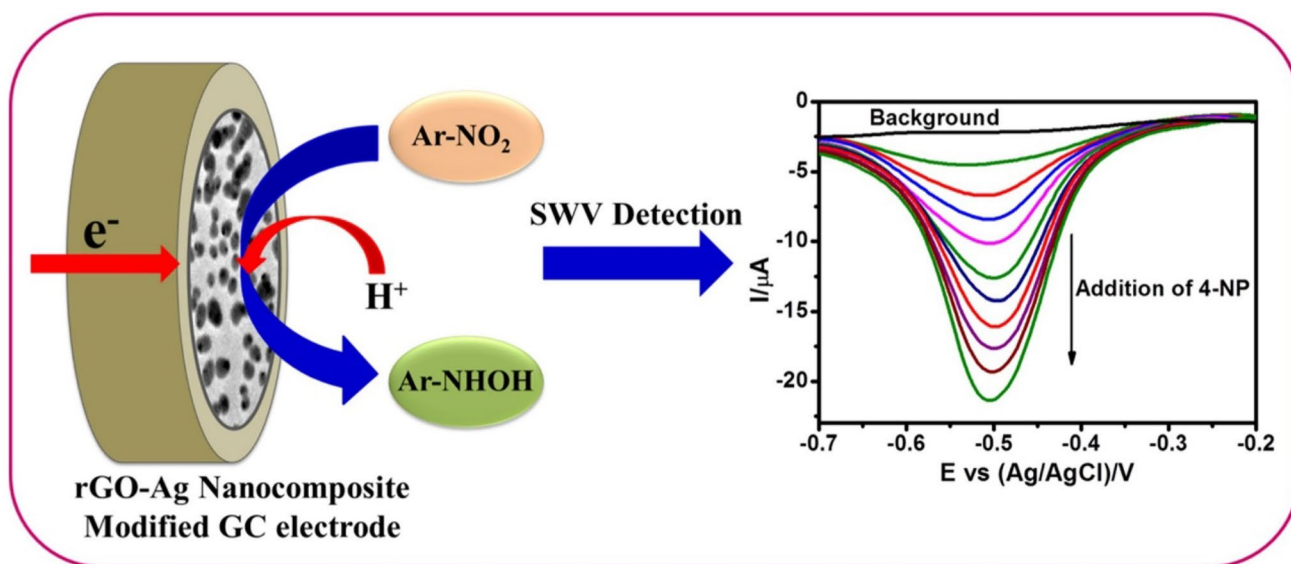


**Fig. 10** Scheme of the detection of 4-NP on rGO@AgNPs (reproduced with permission from Copyright Elsevier Ref. [99])

A multi-functional magnetically separable core–shell structured tannic acid (TA)-coated iron oxide nanosphere nanocatalyst was used for the detection and catalytic reduction of 4-nitrophenol [101]. For the reduction of silver ions into AgNPs, the TA@Fe<sub>2</sub>O<sub>3</sub>NPs were utilised as reducing and stabilising agents. The hydroxyl and ketonic groups in the Fe<sub>2</sub>O<sub>3</sub> nanosphere assisted in the immobilisation of the active catalytic species on the electrode surface. A low reduction potential (−0.39 V) was obtained for the quantification of 4-NP using TA@Fe<sub>2</sub>O<sub>3</sub>NPs@AgNPs/GCE, and it was effectively used in the quantification of 4-nitrophenol in tap water, river water, and drinking water. The catalytic reduction of 4-NP took 7 min in the presence of sodium borohydride.

The schematic of the detection and catalytic reduction of 4-NP is shown in Fig. 11.

In another investigation, silver amalgam particles (AgAPs) were electrodeposited on a pyrolytic graphite electrode (PGE) to detect 4-nitrophenol electrochemically [102]. SEM, energy-dispersive X-ray spectroscopy, image processing software, and cyclic voltammetry were used to optimise the surface shape, resultant composition, and electrochemical characteristics of AgAPs. In addition, UV–Vis chronoamperometry was employed to gain significant information on the reduction rate constant and the number of electron exchanges at the working electrode interface. Because of the electrodeposition route used in sensor preparation, the sensor was stable.

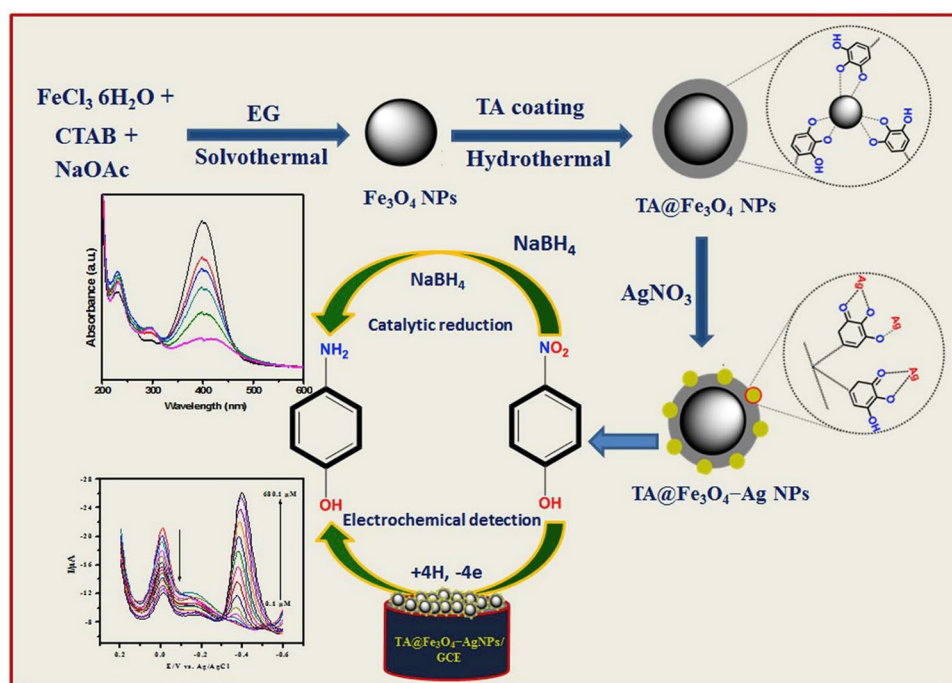
As a host matrix, a functionalised metal–organic framework (MOF) was employed to encapsulate silver–palladium

bimetallic nanoparticles for electrochemical detection and catalytic reduction of 4-NP [103]. The sensor demonstrated amazing analytical qualities such as high specific surface area, high conductivity, and quick electron transfer capabilities. Using tap water samples, the practical applicability of the constructed sensor was evaluated with satisfactory recoveries. The nanocatalyst was used to catalyse the reduction of 4-NP, and the results proved the outstanding catalytic activity and good recyclability for five consecutive cycles without substantial activity loss.

A one-dimensional (1-D) silver nanowire (AgNW) in conjunction with polyaniline (PANI) was used in the fabrication of the sensor for the quantification of 4-NP [104]. The AgNW was used in the fabrication of the sensor because of its ability to promote efficient electron transfer due to the confinement effect coupled with effective surface exposure at the electrode–electrolyte interface alongside its highly integrated morphological features. The synthesised nanocomposite was dissolved in methanol and cast on the electrode surface to form (AgNWs@PANI/GCE). Different optimisation parameters, including the effect of pH and scan rate studies, were interrogated to examine the electron transfer number, proton transfer number, standard rate constant of the electrode, and electron transfer coefficient. The electrochemical reduction of 4-NP showed a reduction peak at −0.77 V and was linear within the concentration range of 0.6–32 μM, with a detection limit of 52 nM.

Well-exfoliated graphene nanoflakes were assembled on iron tungsten nitride and protonated polymeric structure of

**Fig. 11** Scheme for the synthesis of TA@Fe<sub>2</sub>O<sub>3</sub>NPs@AgNPs and its electrochemical detection and electrocatalytic reduction of 4-NP (reproduced with permission from Copyright Elsevier [101])



PANI [105]. The electrode was modified with (PANI-GO (graphene oxide)-iron tungsten nitride nanocomposite) for the quantification of 4-nitrophenol in aqueous samples via a reproducible and real-time technique. The sensor demonstrated greater sensitivity with increased protonation, with a sensitivity of  $354.92 \mu\text{A } \mu\text{M}^{-1} \text{ cm}^{-2}$  for oxidation and reduction peak currents. The sensor sensitivity was attributed to the synergistic effect and superior adsorptive capacity of hybrid PANI and GO-iron tungsten nitride (G-ITN). The G-ITN provides a large surface area and facilitated an electron migration rate. In addition, hydrogen bonds formed between the functional groups (FGs) of the GO ( $-\text{OH}$  and  $-\text{COOH}$ ) and the FGs of the 4-NP ( $-\text{OH}$  and  $\text{NO}_2$ ), as well as  $\pi$ - $\pi$  stacking in aromatic 4-NP and GO structures, all contributed considerably to the measurement of 4-NP at the nanomolar level.

Molecularly imprinted PANI was used in conjunction with graphene oxide (GO) to determine p-nitrophenol [106]. Notably, ion-imprinting is based on the adsorption of para-nitrophenol and PANI on the GO surface via hydrogen bonding and stack interaction in the presence of sodium dodecyl sulphate (SDS) as an anionic surfactant in an aqueous solution. The polymerisation of aniline monomer on GO sheets in the presence of ammonium persulfate solution as a template molecule produced the nanocomposite. The working electrode (carbon paste electrode) was created by combining the synthesised PANI@GO nanocomposite with graphite and paraffin, then injecting the homogenous paste into a plastic needle-type capillary tube and connecting a copper wire to the measurement system. The prepared smart nanosensor was successfully used in the quantification of p-NP in acetate buffer ( $\text{pH} = 5$ ) with a low detection limit of  $0.02 \text{ mmol/L}$ , which was attributed to the high surface area and the selective binding sites of the nanocomposite (PANI@GO). The drawback of this platform, in our opinion, is based on human error that occurs during the preparation of the homogenous paste and the loading of the nanocomposites inside the tube of the carbon paste electrode, which severely influences the repeatability of the data during electrochemical analysis. In our opinion, the limitation of this platform is based on human error that occurs during the preparation of the homogenous paste, which greatly impacts the repeatability of the results during an electrochemical examination.

In another report, a positively charged poly(diallyl dimethylammonium chloride), PDDA-graphene (PDDA-G) was used as a matrix to anchor the quantification of 4-nitrophenol [107]. The modifier was synthesised by adding GO, PDDA, and hydrazine solution into a Teflon-line autoclave for 3 h at  $100^\circ\text{C}$ . The final product was washed with ultra-pure water and dried in an oven. The sensor was prepared by dissolving PDDA-G in ultrapure water with the help of ultrasonic agitation for 6 h. Afterwards,  $5 \mu\text{L}$  of the

homogeneous black suspension was carefully deposited on the GCE surface to form the sensor (PDDA-G/GCE). The reduction current of 4-NP was enhanced when PDDA-G was deposited on the GCE surface because the pyridine nitrogen in the PDDA skeleton has a strong electron-withdrawing capability, which makes the nitrogen group of 4-NP electron deficient, hence, facilitated the reduction of the analyte on the electrode surface. The electrochemical reduction of 4-NP on the PDDA-G/GCE is a two-electron and two-proton process and was successfully used in the detection of 4-NP in wastewater, yellow river, and tap-water samples with a recovery rate of 99.3 to 104.6%, which agrees with HPLC result. For future studies, co-electrodeposition of the modifiers would be a better approach because most modifiers leach in the analyte solution when they are drop dried on the electrode surface, especially after using the sensor for three to four electrochemical analyses.

An enzymeless PEDOT:poly(styrene sulfonate) (PSS) was used in the development of a smart sensor for the detection of nitrophenols, organophosphorus compounds (diethyl 2,4 dinitrophenyl phosphate (DEDNPP)), and diethyl-4-nitrophenyl phosphate (Paraxon) [108]. The ITO electrode was prepared using a chronoamperometry technique by using a potential of  $1.25 \text{ V}$  and a deposition charge of  $15 \text{ m cm}^{-2}$  in a solution containing  $10 \text{ mmol L}^{-1}$  EDOT and  $0.1 \text{ mmol L}^{-1}$  PSSNa. The results obtained from cyclic voltammetry and UV-vis spectroscopy confirmed that the electrochemical mechanism of the reduction of nitrophenol is based on a condensation reaction, and its isomers were detected by linear sweep voltammetry using the oxidation peak of the intermediates. The sensor was used in the detection of DEDNPP and Paraxon with sensitivities of  $0.1843 \text{ A L}^{-1}$  and  $0.1767 \text{ A L}^{-1}$ , respectively.

Yin et al. coated a thiophene-based microporous polymer film on the surface of GCE for the co-detection of isomers of nitrophenol (o-NP, m-NP, and p-NP) [109]. The poly(1,3,5-tri(thiophene-2yl)benzene (PTTB) microporous polymer was immobilised on the glassy carbon electrode by one-step electropolymerisation without the addition of surfactant. The cyclic voltammetry technique was used to interrogate the electrochemical signature of the nitrophenol isomers on a bare GCE and PTTB/GCE. For the bare GCE, all the isomers of nitrophenols gave clear reduction peaks at  $-0.8 \text{ V}$ , which corresponds to the irreversible reduction of the nitro-group. Hence, it is impossible to simultaneously detect the isomers of nitrophenol on this platform. Interestingly, the modified electrode gave clear oxidation-reduction peaks for all the isomers ( $0.263$  and  $0.211 \text{ V}$  for o-NP,  $0.000$  and  $-0.058 \text{ V}$  for m-NP, and  $0.163$  and  $0.128 \text{ V}$  for p-NP). The reasons for the distinguished oxidation-reduction peaks of the isomers were attributed to the significant enhancement in the surface area of the electrode, which increases the contact areas

of the analytes. Also, the strong interaction between the electron-rich thiophene-based microporous polymers and electron-poor nitro analytes considerably improved the electron migration process and improved the adsorption capability. Hence, the electrochemical signals of all the nitrophenol isomers were significantly boosted.

In another study, bimetallic oxides of iron and titanium ( $\text{FeO}_x/\text{TiO}_2$ ) were incorporated into the matrix of mesoporous carbon (MC) for the sensitive and selective determination of 4-NP [110]. The nanocomposite was prepared by direct pyrolysis of a bimetallic Fe/Ti-based metal–organic framework at different temperatures (500 °C, 700 °C, and 900 °C). The composite ( $\text{FeO}_x/\text{TiO}_2@MC$ ) possesses a large specific surface area ( $158.2 \text{ m}^2\text{g}^{-1}$ ), surplus active sites, and fast electron transfer. These analytical qualities played significant roles in the quantification of 4-NP in the river and tap samples using amperometry techniques. The average recoveries range achieved were 95.9 to 103.0% and 103.7 to 108.7% for river and tap water samples, respectively.

Magnetite-platinum nanoparticles were synthesised and used for individual and simultaneous detection of isomers of 2-, 3-, and 4-nitrophenol [111]. During the preparation of the nanocomposite, *n*-propyl-4-picoline silsesquioxane chloride was used as a stabilising agent to infuse the two metallic nanoparticles and assisted in the separation of the nitrophenol isomers. The sensor was used for the detection of 2-, 3-, and 4-nitrophenol in rain and water samples. The rain sample was collected in July 2016 and stored at 7 °C, while the urine samples were collected from a healthy 25-year-old man and stored at the same temperature. During analysis, 10 mL of the urine sample was centrifuged for 600 s at 2000 rpm; the supernatant was filtered and spiked with 11 and  $16 \mu\text{mol L}^{-1}$  concentrations of the isomers. The isomers with acceptable recovery rates were quantified using the conventional standard addition method.

A novel magnetic covalent organic framework (COF) was used as an electrocatalyst for the simultaneous detection of *p*-nitrophenol (PNP) and *o*-nitrophenol (ONP) [112]. It is quite challenging to prepare COF that is suitable for the simultaneous detection of the analytes due to the difficulty in manipulating its composition, dimension, and morphology with surplus active sites. Hence,  $\text{Fe}_3\text{O}_4$  nanoparticles with surface morphological structure, good water dispersity, high surface area, and excellent conductivity were networked into the matrix of COF for the electrochemical detection of *p*-nitrophenol and *o*-nitrophenol. The prepared  $\text{Fe}_3\text{O}_4@COF$ -based electrochemical sensor was successfully used for the co-detection of PNP and ONP with a wide linear concentration range of 10–300  $\mu\text{M}$  and detection limits of 0.2361 and 0.6568  $\mu\text{M}$  were obtained.

Nanoporous gold (NG) with uniform pore sizes was synthesised and used for the electrochemical detection of

PNP [113]. The NG was synthesised by dealloying, and its electrochemical behaviour differed from that of the polycrystalline gold electrode because its cyclic voltammogram revealed a pair of approximately symmetric redox waves attributable to the reaction of the 4-(hydroxyl amino) phenol/4-nitrophenol couple. The NG was prepared by selectively dissolving the silver component of Au–Ag alloys in corrosive conditions, and it possesses a high surface-to-volume ratio as well as excellent porosity. These qualities were important in detecting trace PNP in wastewater. By applying a voltage of 1.0 V for 10 s, the nanoporous gold electrode can be cleaned and reused.

Nitrogen-doped carbon spheres in conjunction with gold nanoparticles (AuNPs) were used to simultaneously detect trace nitrophenol and dihydroxybenzene [114]. Poly(dopamine) (PDA) nanocomposite was prepared by dispersing it in deionised water. Following that, aqueous  $\text{HAuCl}_4$  was added and mixed for 24 h at room temperature. The resultant PDA-AuNP was carefully cleaned with deionised water and oven dried at 60 °C for half a day. C/N-AuNPs were produced by calcining the nanocomposite at various temperatures for 120 min in a boiler at a heating rate of  $1 \text{ }^\circ\text{C min}^{-1}$ . The nanocomposite was dispersed in DMF and 0.05 wt% Nafion to make the sensor. Afterwards, 10  $\mu\text{L}$  of the resulting solution was drop dried on the glassy carbon electrode at ambient temperature to form C/N-AuNPs@GCE. This platform was used for the detection of nitrophenol at low concentrations because of the conversion of nitrophenol to aminophenol (AMP). The AMP formed was covalently bonded to AuNPs on the electrode surface. It is noteworthy to highlight that the electrochemical redox of PNP, ONP, and *m*-nitrophenol is a two-proton and two-electron process. For future studies, it is recommended that the synthesised C/N-AuNPs should be co-electrodeposited on the electrode surface rather than drop drying the nanocomposite on GCE. The electrodeposition method would have enhanced the sensor's sensitivity and stability.

Au–CuNP bimetallic alloy nanoparticles were used in the development of electrochemical sensors for the detection and electrochemical reduction of nitroarenes [115]. These metals were coupled together with the understanding that bimetallic nanoparticles possess superior catalytic selectivity, electrocatalytic activity, high surface area, and physical and chemical properties than single-metal analogues owing to the synergistic effects from both metals. The nanoparticles were synthesised individually and collectively. Different ratios (1:1, 1:2, and 1:3) of the bimetallic nanoparticles (Au:Cu) were prepared. The results obtained from the electrochemical impedance spectroscopy studies revealed that the AuNPs are more conductive than the CuNPs and the 1:3 (Au–Cu) gave the lowest charge transfer resistance and highest peak current signal. Hence, it was used in the electrochemical detection and electrocatalytic reduction of 4-nitrophenol,

2-methyl-3-nitrophenyl acetic, 2, amino-4-nitrophenol, and 3-nitrotoluene. The results obtained from electrochemical studies were validated with computation studies using density functional methods. Ionisation potential, electronegativity, and electrophilicity were calculated, and the results were consistent with the experimental data.

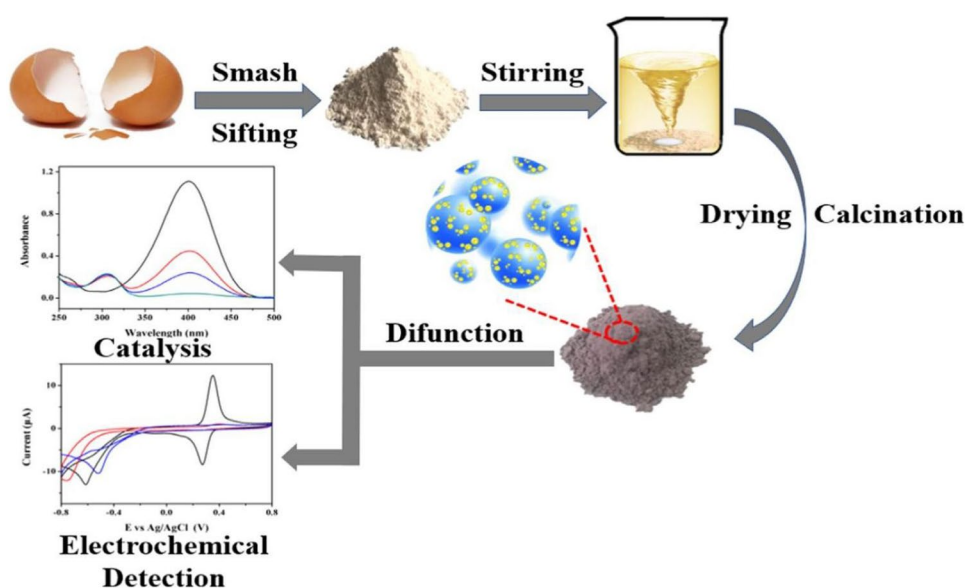
Ding and his co-workers converted waste eggshells into difunctional Au/CaCO<sub>3</sub> nanocomposite for the catalytic reduction and electrochemical detection of 4-nitrophenol [116]. The fresh eggshell was washed with ultrapure water to remove any trace of impurities and dried for 5 h in an oven to remove moisture from its surface. With a 200-mesh sieve, the eggshell was ground and sieved to a fine powder. The eggshell powder was added to a chloroauric acid solution and stirred for 12 h before being calcined in a tube furnace at 500 °C for 120 min at a heating rate of 2 °C/min. Using cyclic voltammetry and chronoamperometric methods, the Au/CaCO<sub>3</sub> nanocomposite was effectively employed to determine 4-nitrophenol. Furthermore, the Au/CaCO<sub>3</sub> nanocomposite was employed as a smart nanocatalyst for the effective reduction of 4-NP, demonstrating outstanding stability and activity. At a  $K$  value of 1.0750 min<sup>-1</sup>, the catalytic process followed the pseudo-first-order kinetic model. The overall scheme for the detection and catalytic reduction of 4NP is shown in Fig. 12.

A comparative study between CeO<sub>2</sub>-CuO and CeO<sub>2</sub>-CuO/CS nanocomposites for the detection and catalytic removal of 4NP was investigated by Khan et al. [117]. Both nanocomposites were used in the construction of sensors for 4NP. The results of the cyclic voltammogram demonstrated that when the concentration of 4NP increased from a concentration range of 74–390 μM, there was a gradual improvement in the peak current signal. The CeO<sub>2</sub>-CuO/CS nanocomposites gave a lower detection limit of 2.03 μM than the 2.85 μM obtained

from CeO<sub>2</sub>-CuO nanocomposite. Due to this, CeO<sub>2</sub>-CuO/CS nanocomposite was employed as a nanocatalyst for the conversion of 4-NP to 4-aminophenol in the presence of sodium borohydride. The reaction rate ( $K_{app}$ ) constants obtained from the plot of  $\ln(C_t/C_0)$  were -0.0110 min<sup>-1</sup>, -0.0290 min<sup>-1</sup>, -0.05133 min<sup>-1</sup>, and -0.1012 min<sup>-1</sup>. These results provided additional evidence of the CeO<sub>2</sub>-CuO/CS nanocomposite catalytic effectiveness in the reduction of 4NP.

Cerium-oxide-cobalt oxide-chitosan (CH/CeO<sub>2</sub>-Co<sub>2</sub>O<sub>3</sub>) nanocomposite was coated on pencil graphite-graphite lead electrode (PGL) and glassy carbon electrode for the electrochemical detection of nitrophenols (2, nitrophenol, 4-nitrophenol, and 2,6-dinitrophenol) using cyclic voltammetry [118]. Cerium nitrate and cobalt nitrate were stirred together in deionised water to form the CeO<sub>2</sub>-Co<sub>2</sub>O<sub>3</sub> nanocomposite and NaOH was then used to raise the pH to 10 at 60 °C. The resulting solution was cooled, washed, dried, and calcined at 500 °C. Meanwhile, the CH/CeO<sub>2</sub>-Co<sub>2</sub>O<sub>3</sub> nanocomposite was prepared by dispersing CeO<sub>2</sub>-Co<sub>2</sub>O<sub>3</sub> in a chitosan solution, and formaldehyde was added slowly to form the chitosan hydrogel. The CC/CH/CeO<sub>2</sub>-Co<sub>2</sub>O<sub>3</sub> was prepared by immersing a piece of cotton cloth (CC) in the CH/CeO<sub>2</sub>-Co<sub>2</sub>O<sub>3</sub> solution and kept dry at 25 °C. The sensors (Nafion/CeO<sub>2</sub>-Co<sub>2</sub>O<sub>3</sub> and Nafion/CeO<sub>2</sub>-Co<sub>2</sub>O<sub>3</sub>/PGL) were used for the detection of 4NP, and the results obtained revealed that the Nafion/CeO<sub>2</sub>-Co<sub>2</sub>O<sub>3</sub>/PGL produced higher peak current signal than the Nafion/CeO<sub>2</sub>-Co<sub>2</sub>O<sub>3</sub>; this enhancement was attributed to the electron transfer, excellent redox properties, and catalytic potential of Nafion/CeO<sub>2</sub>-Co<sub>2</sub>O<sub>3</sub> towards the reduction of 4NP as well as the higher conductivity of PGL over GCE. Additionally, the 4-nitrophenol was catalytically reduced to 4-aminophenol for 9 min using the CC/CH/CeO<sub>2</sub>-Co<sub>2</sub>O<sub>3</sub> nanocomposite. Notably, the CC helped remove the catalyst from the reactor

**Fig. 12** Schematic of the synthesis and application of Au/CaCO<sub>3</sub> nanocomposite for the detection and catalytic reduction of 4NP (reproduced with permission from Copyright Elsevier Ref. [116])



and increased the catalytic activity of the nanocatalyst. Due to their higher sensitivity, we believe that differential pulse voltammetry or square wave voltammetry should be used instead of cyclic voltammetry for electrochemical study.

Hydrothermal production of spinel mesoporous  $\text{ZnCo}_2\text{O}_4$  nanosheets was employed to alter GCE for the simultaneous and individual detection of *o*-nitrophenol and *p*-nitrophenol [119].  $\text{Zn}(\text{NO}_3)_2 \cdot 6\text{H}_2\text{O}$ ,  $\text{Co}(\text{NO}_3)_2 \cdot 6\text{H}_2\text{O}$ , and urea were dissolved in distilled water to form the meso- $\text{ZnCo}_2\text{O}_4$  nanosheets, which were then placed in a Teflon-lined autoclave for 12 h at 160 °C. The meso- $\text{ZnCo}_2\text{O}_4$  nanosheets were prepared by dissolving  $\text{Zn}(\text{NO}_3)_2 \cdot 6\text{H}_2\text{O}$ ,  $\text{Co}(\text{NO}_3)_2 \cdot 6\text{H}_2\text{O}$ , and urea in distilled water and the resulting solution was transferred into a Teflon-lined autoclave at 160 °C for 12 h. The  $\text{ZnCo}_2\text{O}_4$  nanosheet was coated on the GCE and Nafion solution was dropped on it to prevent the leaching of the nanosheets into the analyte solution. Several optimisation factors were investigated, including

the pH of the phosphate buffer solution, scan rate, and concentration of the meso- $\text{ZnCo}_2\text{O}_4$  dispersion. The results of the optimisation investigation showed that, when the pH value increased from 5.0 to 9.0, the cathodic peak current shifted to the negative potential and showed linear correlations, confirming that protons were involved in the reaction processes. The mechanism of the electrochemical process involved the reduction of nitrophenol to hydroxy amino phenol with four-electron and four-proton transfer steps. During the simultaneous detection of the analytes, the peak separation potential was  $-0.636$  V and  $-0.762$  V at a concentration range of 1–4000  $\mu\text{M}$ . Low sensitivities of 0.256 and 0.318  $\mu\text{A } \mu\text{M}^{-1} \text{cm}^{-2}$  were obtained for both analytes, which was attributed to the large specific area, catalytic active sites, and excellent physicochemical properties of the mesoporous  $\text{ZnCo}_2\text{O}_4$  nanosheets. Figure 13 shows the detection limit of simultaneous detection and individual detection of the analytes.

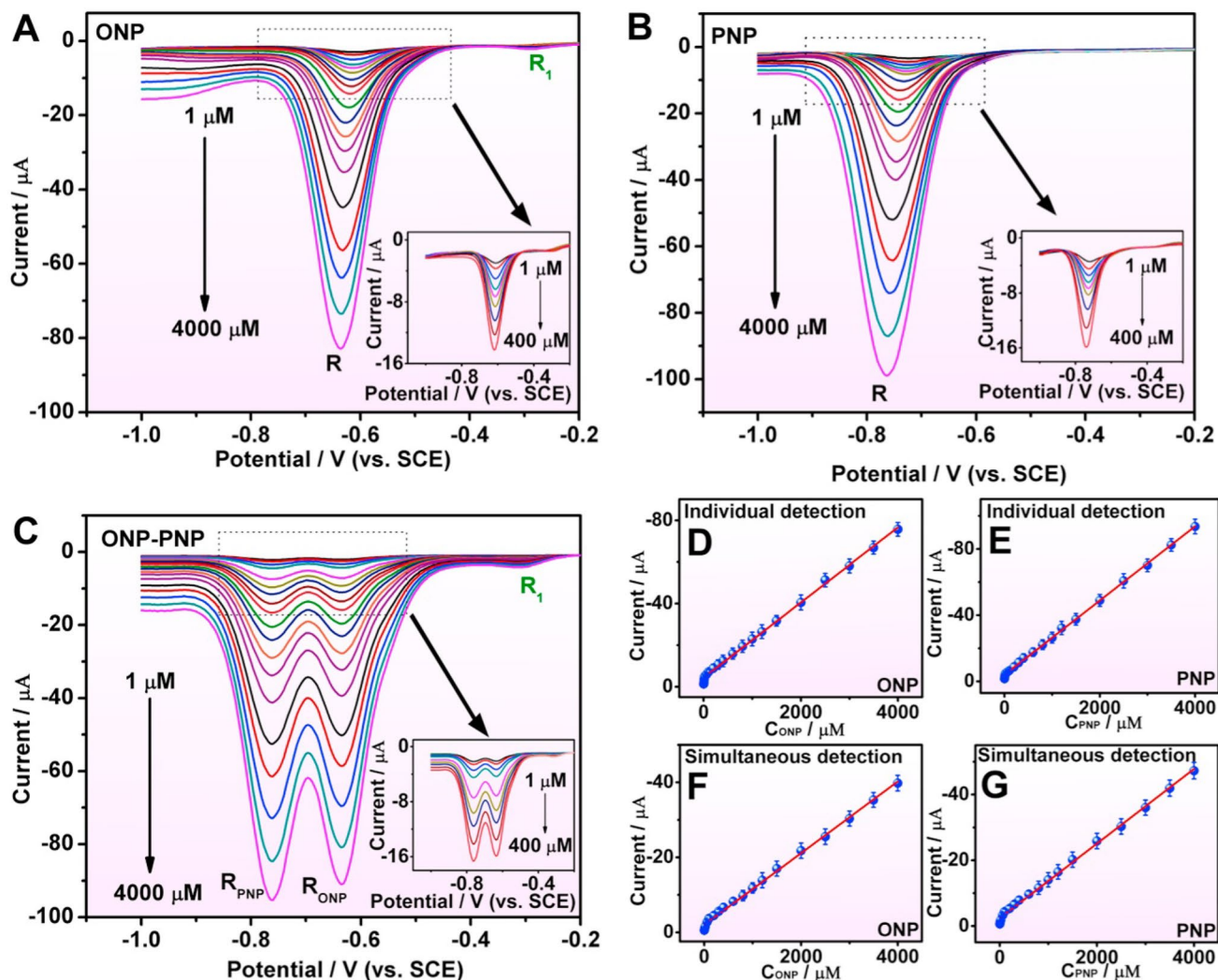


**Fig. 13** **A, B** DPV for the detection of ONP and PNP using meso- $\text{ZnCo}_2\text{O}_4/\text{GCE}$ . **C** Co-detection of the analytes. **D–G** Calibration plots of the reduction current against the concentration of ONP and PNP (reproduced with permission from Copyright Elsevier (2020) Ref [119])

Balram and his colleagues coated functionalised multi-walled carbon nanotubes (*f*MWCNTs) with a 3D flower-zinc oxide for the detection of 4-NP [120]. The laser-assisted method was used to create the 3D flower-like ZnNP, and the ultrasonication method was used to create the nanocomposite ZnNP@*f*MWCNTs utilising a high-intensity ultrasonic bath with a frequency of 40 kHz and 200 W/cm<sup>2</sup> power. To create ZnNP@*f*MWCNTs/SPCE, the resulting nanocomposite was disseminated in ethanol using an ultrasonication process and carefully dropped cast on a screen-printed carbon electrode (SPCE). Additional electrodes, such as ZnNPs/SPCE and *f*MWCNTs/SPCE, were made in the same way. The electrochemical evaluation of the electrodes revealed that ZnNPs@*f*MWCNTs/SPCE produced the best electrochemical signal, followed by *f*MWCNTs/SPCE and ZnNPs/SPCE. This was attributable to the increased surface area combined with the synergistic action of ZnO NPs and *f*MWCNTs. As a result, the author employed ZnNPs@*f*MWCNTs/SPCE to detect 4-NP utilising differential pulse voltammetry (DPV). The findings revealed that the electrochemical mechanism of 4-NP involved the reduction of 4-NP to 4-hydroxy aminophenol (4-HAP) and subsequent redox conversion to 4-nitrosophenol. The electrode detected 4-NP in tap and river water using the standard addition method, with a recovery rate ranging from 99.33 to 101.33%. Square wave voltammetry should be employed in future investigations since it is more sensitive than differential pulse voltammetry.

MWCNTs were enveloped around hierarchical MnO<sub>2</sub> nanoflakes for electrochemical detection of p-nitrophenol [121]. The MnO<sub>2</sub> nanoflakes were wrapped on the MWCNTs, according to the image obtained from the high-resolution transmission electron microscopy (HRTEM). The crystallinity of the nanocomposite was demonstrated by the selected area electron diffraction pattern (SAED). The amperometry technique with a working potential of −0.95 V was utilised to detect PNP at the micro-molar level. The current increases proportionally to the analyte concentration, and the sensor's sensitivity was estimated using the slope of the calibration plot/area of the electrode (0.14 cm<sup>2</sup>). The sensor's sensitivity and detection limit were 0.186 A M<sup>−1</sup> cm<sup>−2</sup> and 0.64 μM, respectively.

In general, sensor construction can be illustrated in Fig. 14. The conducting substrate could be a glassy carbon electrode, a screen-printed electrode, an exfoliated graphite electrode, a fluorine-doped tin-oxide electrode, or a gold electrode, and various nanomaterials such as inorganic and organic nanomaterials are used to improve electrochemical communication on the conducting substrate. After immobilising the nanomaterials on the conducting substrate via drop drying, spin coating, drop casting, or electrodeposition method, the sensor is used as the working electrode in a three-electrode system, including counter, and reference electrode. The counter electrode permits charge flow, the reference electrode provides a constant and defines potential, and the working electrode is where

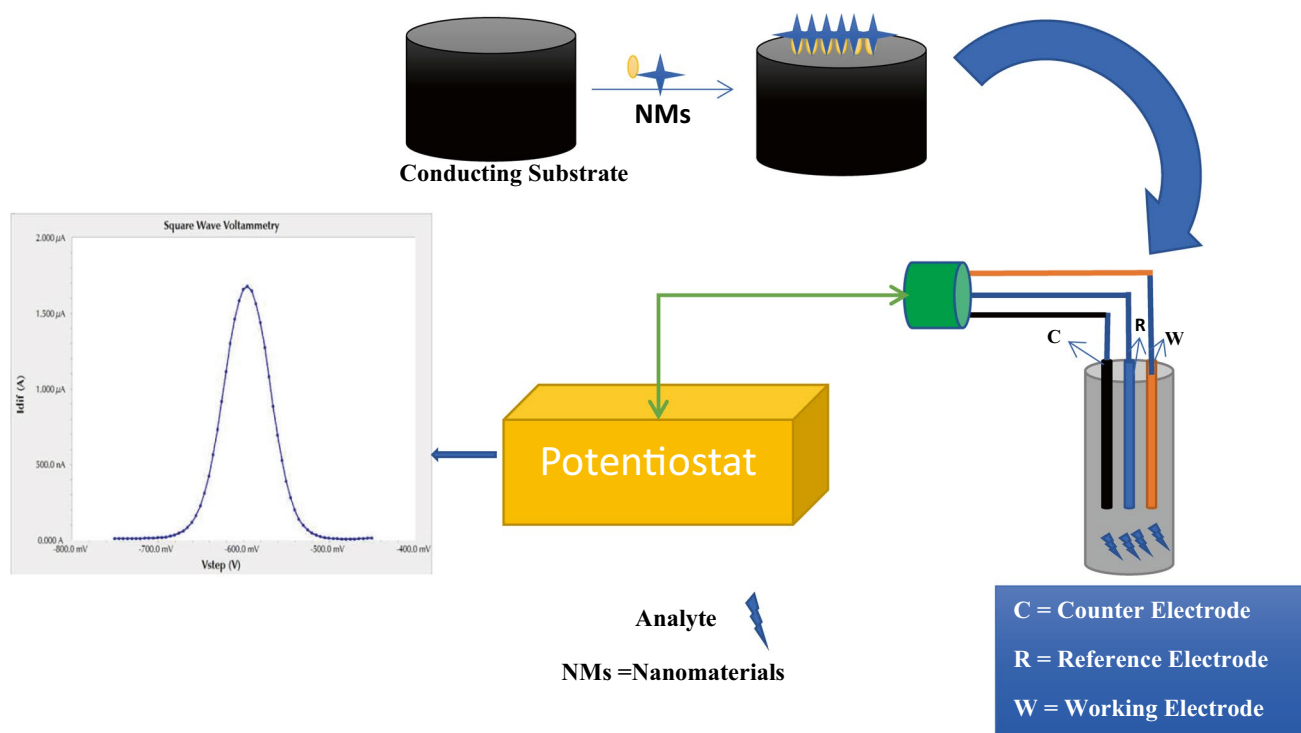


**Fig. 14** A simple electrochemical set-up for the detection of analytes using electrochemistry approach

the major electrochemical reaction takes place. To mention a few, cyclic voltammetry, differential pulse voltammetry, square wave voltammetry, electrochemical impedance spectroscopy, chronoamperometry, and amperometry can be used to analyse the electrochemical signal produced by the sensor during electroanalysis. The simplicity of electrochemical techniques is a significant underpinning of their widespread applicability.

## Conclusion and Future Outlooks

The synthesis of several smart nanomaterials and their applications in the modification of various conducting substrates for the electrochemical detection of toxic organic pollutants has been discussed. The application of nanomaterials for the development of electrochemical sensors helps to overcome the sluggish electron transfer, electrode fouling, high background current, and poor detection limit that occurred using an un-modified electrode. Different important analytical properties of the nanomaterials such as catalytic, mechanical, optical, chemical, and magnetic properties played considerable roles in improving the sensitivity of the sensor. It is noteworthy to highlight that nanomaterials played crucial roles in the detection and electrocatalytic reduction of organic pollutants in various matrices. It is crucial to emphasise that ecologically friendly synthetic approaches should be employed in the preparation of nanomaterials, and inexpensive precursors should be used to lower sensor costs.

It is also critical to consider the electrode platform employed in sensor development. We recommended screen-printed electrodes because their design prevents modifiers from leaching into analytical solutions and allows them to interact with analyte solutions more easily. As a result, this electrode can be utilised to analyse real-world samples without jeopardising the electrochemical signal's integrity. Furthermore, the aptasensors approach is a smart methodology that may be used to tackle sensor interference difficulties during organic pollutant detection. Hydrophobic or anti-electrode passivation nanomaterials such as polyoxometalates, chitosan, nickel oxide, or diamond can be used to address the problem of electrode fouling during organic pollutant detection. Nanomaterials should be immobilised on conducting substrates using an electrodeposition method to prevent nanomaterial leaching in the analyte solution, and at least two electrochemical techniques be used in analyte detection. Additionally, if the electrodeposition method is not used, Nafion or an eco-friendly binding agent must be used in the sensor development.

Although remarkable progress has been made in the electrochemical detection of organic pollutants, most of the reports documented in the literature were not used for industrial applications. We recommend that sensors

prepared via electrodeposition be incorporated into reactors for water treatment because sensors prepared via this platform produce consistent and reproducible results.

**Author Contribution** Azeez Olayiwola Idris: conception and design of study; acquisition of data; analysis and/or interpretation of data; drafting the manuscript; Benjamin Orimolade: conception and design of study; acquisition of data; analysis and/or interpretation of data; drafting the manuscript; Lynn Dennany: revising the manuscript critically for important intellectual content and proofreading; Bhekhe Mamba: revising the manuscript critically for important intellectual content and proofreading; Shohreh Azizi: conception and design of study; acquisition of data; analysis and/or interpretation of data; K. Kaviyarasu: conception and design of study; acquisition of data; analysis and/or interpretation of data; Malik Maaza: conception and design of study; acquisition of data; revising the manuscript critically for important intellectual content; funding acquisition.

**Funding** Open access funding provided by University of South Africa. The robust assistance of the National Research Foundation (NRF), South Africa (grant number: 145431), is fully recognised and exceptionally appreciated.

National Research Foundation, 145431

**Availability of Data and Materials** Not applicable.

## Declarations

**Ethical Approval** Not applicable.

**Competing Interests** The authors declare no competing interests.

**Open Access** This article is licensed under a Creative Commons Attribution 4.0 International License, which permits use, sharing, adaptation, distribution and reproduction in any medium or format, as long as you give appropriate credit to the original author(s) and the source, provide a link to the Creative Commons licence, and indicate if changes were made. The images or other third party material in this article are included in the article's Creative Commons licence, unless indicated otherwise in a credit line to the material. If material is not included in the article's Creative Commons licence and your intended use is not permitted by statutory regulation or exceeds the permitted use, you will need to obtain permission directly from the copyright holder. To view a copy of this licence, visit <http://creativecommons.org/licenses/by/4.0/>.

## References

1. H. Ji, D. Peng, C. Fan, K. Zhao, Y. Gu, Y. Liang, Assessing effects of non-point source pollution emission control schemes on Beijing's sub-center with a water environment model. *Urban Climate* **43**, 1–12 (2022)
2. R.S. Ahmed, M.E. Abuarab, M.M. Ibrahim, M. Baioumy, A. Mokhtar, Assessment of environmental and toxicity impacts and potential health hazards of heavy metals pollution of agricultural drainage adjacent to industrial zones in Egypt. *Chemosphere* **318**, 1–15 (2023)
3. T.S. Hamidon, M.H. Hussin, Improved p-chlorophenol adsorption onto copper-modified cellulose nanocrystal-based hydrogel spheres. *Int. J. Biol. Macromol.* **233**, 1–11 (2023)
4. K. Czarny-Krzyminińska, B. Krawczyk, D. Szczukocki, Bisphenol A and its substitutes in the aquatic environment: occurrence and toxicity assessment. *Chemosphere* **315**, 1–26 (2023)

5. K. Baralić, K. Živančević, D. Javorac, A. Buha Djordjevic, M. Anđelković, D. Jorgovanović, Multi-strain probiotic ameliorated toxic effects of phthalates and bisphenol A mixture in Wistar rats. *Food Chem. Toxicol.* **143**(6), 1–15 (2020)
6. M.K. Abugazleh, B. Rougeau, H. Ali, Adsorption of catechol and hydroquinone on titanium oxide and iron (III) oxide. *J. Environ. Chem. Eng.* **8**(5), 1–9 (2020)
7. A. Umar, A.A. Ibrahim, R. Kumar, T. Almas, P. Sandal, M.S. Al-Assiri, Fern shaped La<sub>2</sub>O<sub>3</sub> nanostructures as potential scaffold for efficient hydroquinone chemical sensing application. *Ceram. Int.* **46**(4), 5141–5148 (2020)
8. P. Benjwal, R. Sharma, K.K. Kar, Effects of surface microstructure and chemical state of featherfiber-derived multidoped carbon fibers on the adsorption of organic water pollutants. *Mater. Des.* **110**(16), 762–774 (2016)
9. E. Lipczynska-Kochany, Humic substances, their microbial interactions and effects on biological transformations of organic pollutants in water and soil: a review. *Chemosphere* **202**(17), 420–437 (2018)
10. I. Adeyemi, R. Sulaiman, M. Almazroui, A. Al-Hammadi, I.M. AlNashef, Removal of chlorophenols from aqueous media with hydrophobic deep eutectic solvents: Experimental study and COSMO RS evaluation. *J. Mol. Liq.* **311**(17), 1–11 (2020)
11. Y. Liu, Q. Wang, S. Guo, P. Jia, Y. Shui, S. Yao, Highly selective and sensitive fluorescence detection of hydroquinone using novel silicon quantum dots. *Sens. Actuators B Chem.* **275**(16), 415–421 (2018)
12. G. Russo, F. Barbato, D.G. Mita, L. Grumetto, Occurrence of bisphenol A and its analogues in some foodstuff marketed in Europe. *Food Chem. Toxicol.* **131**(13), 1–14 (2019)
13. I. Pacheco-Fernández, A. Najafi, V. Pino, J.L. Anderson, J.H. Ayala, A.M. Afonso, Utilization of highly robust and selective crosslinked polymeric ionic liquid-based sorbent coatings in direct-immersion solid-phase microextraction and high-performance liquid chromatography for determining polar organic pollutants in waters. *Talanta* **158**(13), 125–133 (2016)
14. Y. Moliner-Martínez, C. Molins-Legua, J. Verdú-Andrés, R. Herráez-Hernández, P. Campíns-Falcó, Advantages of monolithic over particulate columns for multiresidue analysis of organic pollutants by in-tube solid-phase microextraction coupled to capillary liquid chromatography. *J. Chromatogr. A* **1218**(37), 6256–6262 (2011)
15. M. Levy, J. Al-Alam, O. Delhomme, M. Millet, An integrated extraction method coupling pressurized solvent extraction, solid phase extraction and solid-phase micro extraction for the quantification of selected organic pollutants in air by gas and liquid chromatography coupled to tandem mass spectrometry. *Microchem. J.* **157**(22), 1–9 (2020)
16. J. Fang, H. Zhao, Y. Zhang, M. Lu, Z. Cai, Atmospheric pressure chemical ionization in gas chromatography-mass spectrometry for the analysis of persistent organic pollutants. *Trends Environ. Anal. Chem.* **25**(14), 1–11 (2020)
17. F. Chen, L. Zhao, W. Yu, Y. Wang, H. Zhang, L.H. Guo, Dynamic monitoring and regulation of pentachlorophenol photodegradation process by chemiluminescence and TiO<sub>2</sub>/PDA. *J. Hazard. Mater.* **399**(31), 1–9 (2020)
18. A. Ballesteros-Gómez, F.J. Ruiz, S. Rubio, D. Pérez-Bendito, Determination of bisphenols A and F and their diglycidyl ethers in wastewater and river water by coextractive extraction and liquid chromatography-fluorimetry. *Anal. Chim. Acta* **603**(1), 51–59 (2007)
19. V.A. Muckoya, A.O. Idris, P.N. Nomngongo, J.C. Ngila, Synthesized carbon nanodots for simultaneous extraction of personal care products and organophosphorus pesticides in wastewater samples prior to LC-MS/MS determination. *Anal. Bioanal. Chem.* **411**(23), 6173–6187 (2019)
20. A.O. Idris, N. Mabuba, O.A. Arotiba, Electroanalysis of selenium in water on an electrodeposited gold-nanoparticle modified glassy carbon electrode. *J. Electroanal. Chem.* **758**(18), 7–11 (2015)
21. A.O. Idris, Nonhlangabezo Mabuba, O.A. Arotiba, Towards cancer diagnostics – an a-feto protein electrochemical immunosensor on a manganese (IV) oxide/gold nanocomposite immobilisation layer. *RSC Adv.* **8**(24), 30683–30691 (2018)
22. A.O. Idris, N. Mabuba, O.A. Arotiba, An alpha-fetoprotein electrochemical immunosensor based on a carbon/gold bi-nanoparticle platform. *Anal. Methods* **10**(47), 5649–5658 (2018)
23. C. Rinaldi, D.K. Corrigan, L. Dennany, R.F. Jarrett, A. Lake, M.J. Baker, Development of an Electrochemical CCL17/TARC Biosensor toward rapid triage and monitoring of classic hodgkin lymphoma. *ACS Sens.* **6**(9), 3262–3272 (2021)
24. K. Guo, Advances in the detection of rheumatoid arthritis related biomarker by highly sensitive electrochemical sensors. *Int. J. Electrochem. Sci.* **18**, 1–7 (2023)
25. A.O. Idris, J.P. Mafa, N. Mabuba, O.A. Arotiba, Nanogold modified glassy carbon electrode for the electrochemical detection of arsenic in water. *Russ. J. Electrochem.* **53**(2), 190–197 (2017)
26. S. Vinoth, P. Sampathkumar, K. Giribabu, A. Pandikumar, Ultrasonically assisted synthesis of barium stannate incorporated graphitic carbon nitride nanocomposite and its analytical performance in electrochemical sensing of 4-nitrophenol. *Ultrason. Sonochem.* **2020**(62), 1–10 (2019)
27. C. Liu, X. Bo, L. Guo, A novel electrochemical sensing platform of JUC-62 metal-organic framework / platelet ordered mesoporous carbon for high selective detection of nitro-aromatic compounds. *Sens. Actuators B Chem.* **297**(26), 1–12 (2019)
28. A.B. Zeidman, O.M. Rodriguez-Narvaez, J. Moon, E.R. Bandala, Removal of antibiotics in aqueous phase using silica-based immobilized nanomaterials: a review. *Environ. Technol. Innov.* **20**(9), 1–15 (2020)
29. A.A. Nayl, A.I. Abd-Elhamid, A.Y. El-Moghazy, M. Hussin, M.A. Abu-Saied, A.A. El-Shanshory et al., The nanomaterials and recent progress in biosensing systems: a review. *Trends Environ. Anal. Chem.* **26**(29), 1–14 (2020)
30. X. Mu, J. Liu, L. Yuan, Y. Huang, L. Qian, C. Wang, The pigmentation interference of bisphenol F and bisphenol A. *Environ. Pollut.* **266**(4), 1–10 (2020)
31. K.L. Oguzie, M. Qiao, X. Zhao, E.E. Oguzie, V.O. Njoku, G.A. Obodo, Oxidative degradation of Bisphenol A in aqueous solution using cobalt ion-activated peroxydisulfate. *J. Mol. Liq.* **313**(19), 1–8 (2020)
32. F. Liang, X. Huo, W. Wang, Y. Li, J. Zhang, Y. Feng, Association of bisphenol A or bisphenol S exposure with oxidative stress and immune disturbance among unexplained recurrent spontaneous abortion women. *Chemosphere* **257**(14), 1–7 (2020)
33. Y. Jiang, J. Li, S. Xu, Y. Zhou, H. Zhao, Y. Li et al., Prenatal exposure to bisphenol A and its alternatives and child neurodevelopment at 2 years. *J. Hazard. Mater.* **388**(28), 1–7 (2020)
34. S. Jiang, H. Liu, S. Zhou, X. Zhang, C. Peng, H. Zhou et al., Association of bisphenol A and its alternatives bisphenol S and F exposure with hypertension and blood pressure: a cross-sectional study in China. *Environ. Pollut.* **257**(25), 1–9 (2020)
35. E.A.S. Musachio, S.M. Araujo, V.C. Bortolotto, C.S. de Freitas, M.M.M. Dahleh, M.R. Poetini, Bisphenol A exposure is involved in the development of Parkinson like disease in *Drosophila melanogaster*. *Food Chem. Toxicol.* **137**(9), 1–9 (2020)
36. Y. Liu, Y. Liu, B. Liu, A dual-signaling strategy for ultrasensitive detection of bisphenol A by aptamer-based electrochemical biosensor. *J. Electroanal. Chem.* **781**(1), 265–271 (2016)
37. D. Jemeli, E. Marcoccio, D. Moscone, C. Dridi, F. Arduini, Highly sensitive paper-based electrochemical sensor for reagent free detection of bisphenol A. *Talanta* **216**(14), 1–7 (2020)
38. N. Ben, A. Ait, C. Dridi, A. Amine, Ultrasound assisted magnetic imprinted polymer combined sensor based on carbon black and gold nanoparticles for selective and sensitive

- electrochemical detection of bisphenol A. *Sens. Actuators B Chem.* **276**(4), 304–312 (2018)
39. T.C. Canevari, M.V. Rossi, A.D.P. Alexiou, Development of an electrochemical sensor of endocrine disruptor bisphenol A by reduced graphene oxide for incorporation of spherical carbon nanoparticles. *J. Electroanal. Chem.* **832**(21), 24–30 (2019)
  40. Y. Wang, C. Yin, Q. Zhuang, An electrochemical sensor modified with nickel nanoparticle/nitrogen-doped carbon nanosheet nanocomposite for bisphenol A detection. *J. Alloys Compd.* **827**(14), 1–11 (2020)
  41. V.M. Ekomo, C. Branger, R. Bikanga, A.M. Florea, G. Istamboulie, C. Calas-Blanchard et al., Detection of bisphenol A in aqueous medium by screen printed carbon electrodes incorporating electrochemical molecularly imprinted polymers. *Biosens. Bioelectron.* **112**(9), 156–161 (2018)
  42. T.S. Anirudhan, V.S. Athira, V.C. Sekhar, Electrochemical sensing and nano molar level detection of bisphenol- A with molecularly imprinted polymer tailored on multiwalled carbon nanotubes. *Polymer (Guildf.)* **146**(18), 312–320 (2018)
  43. F. Tan, L. Cong, X. Li, Q. Zhao, H. Zhao, X. Quan et al., An electrochemical sensor based on molecularly imprinted polypyrrole/graphene quantum dots composite for detection of bisphenol A in water samples. *Sens. Actuators B Chem.* **233**(27), 599–606 (2016)
  44. C. Bodin, B. Gelinat, J. Deng, K. Pithaksinsakul, Y. Zhu, D. Rochefort, D. Fontaine, Describing the unsuspected advantage of redox ionic liquids applied to electrochemical energy storage. *Curr. Opin. Colloid Interface Sci.* **64**, 1–11 (2023)
  45. P. Butmee, G. Tumcharern, P. Saejueng, D. Stankovic, A direct and sensitive electrochemical sensing platform based on ionic liquid functionalized graphene nanoplatelets for the detection of bisphenol A. *J. Electroanal. Chem.* **833**(12), 370–379 (2019)
  46. J. Cai, B. Sun, W. Li, X. Gou, Y. Gou, D. Li, Novel nanomaterial of porous graphene functionalized black phosphorus as electrochemical sensor platform for bisphenol A detection. *J. Electroanal. Chem.* **835**(4), 1–9 (2019)
  47. Y. Yang, H. Zhang, C. Huang, N. Jia, MWCNTs-PEI composites-based electrochemical sensor for sensitive detection of bisphenol A. *Sens. Actuators B Chem.* **235**(21), 408–413 (2016)
  48. M.Y. Ali, A.U. Alam, M.M.R. Howlader, Fabrication of highly sensitive bisphenol a electrochemical sensor amplified with chemically modified multiwall carbon nanotubes and  $\beta$ -cyclodextrin. *Sens. Actuators B Chem.* **320**(29), 1–9 (2020)
  49. W.R. Zhao, T.F. Kang, L.P. Lu, F.X. Shen, S.Y. Cheng, A novel electrochemical sensor based on gold nanoparticles and molecularly imprinted polymer with binary functional monomers for sensitive detection of bisphenol A. *J. Electroanal. Chem.* **786**(3), 102–111 (2017)
  50. N. Ben Messaoud, M.E. Ghica, C. Dridi, M. Ben Ali, C.M.A. Brett, Electrochemical sensor based on multiwalled carbon nanotube and gold nanoparticle modified electrode for the sensitive detection of bisphenol A. *Sens. Actuators B Chem.* **253**(26), 513–522 (2017)
  51. B. Deiminiat, G.H. Rounaghi, M.H. Arbab-Zavar, I. Razavipanah, A novel electrochemical aptasensor based on f-MWCNTs/AuNPs nanocomposite for label-free detection of bisphenol A. *Sens. Actuators B Chem.* **242**(9), 158–166 (2017)
  52. L. Zhou, J. Wang, D. Li, Y. Li, An electrochemical aptasensor based on gold nanoparticles dotted graphene modified glassy carbon electrode for label-free detection of bisphenol A in milk samples. *Food Chem.* **162**(24), 34–40 (2014)
  53. I. Razavipanah, G.H. Rounaghi, B. Deiminiat, S. Damirchi, K. Abnous, M. Izadyar, A new electrochemical aptasensor based on MWCNT-SiO<sub>2</sub>@Au core-shell nanocomposite for ultrasensitive detection of bisphenol A. *Microchem. J.* **146**(7), 1054–1063 (2019)
  54. G. Bolat, Y.T. Yaman, S. Abaci, Highly sensitive electrochemical assay for bisphenol A detection based on poly (CTAB)/MWCNTs modified pencil graphite electrodes. *Sens. Actuators B Chem.* **255**(9), 140–148 (2018)
  55. Y. Zhu, C. Zhou, X. Yan, Y. Yan, Q. Wang, Aptamer-functionalized nanoporous gold film for high-performance direct electrochemical detection of bisphenol A in human serum. *Anal. Chim. Acta* **883**(6), 81–89 (2015)
  56. X. Zhang, L. Wu, J. Zhou, X. Zhang, J. Chen, A new ratiometric electrochemical sensor for sensitive detection of bisphenol A based on poly- $\beta$ -cyclodextrin/electroreduced graphene modified glassy carbon electrode. *J. Electroanal. Chem.* **742**(14), 97–103 (2015)
  57. Z. Ye, Q. Wang, J. Qiao, B. Ye, G. Li, Simultaneous detection of bisphenol A and bisphenol S with high sensitivity based on a new electrochemical sensor. *J. Electroanal. Chem.* **854**(14), 1–9 (2019)
  58. Y.H. Pang, Y.Y. Huang, L. Wang, X.F. Shen, Y.Y. Wang, Determination of bisphenol A and bisphenol S by a covalent organic framework electrochemical sensor. *Environ. Pollut.* **263**(18), 1–9 (2020)
  59. Q. Li, H. Li, G.F. Du, Z.H. Xu, Electrochemical detection of bisphenol A mediated by [Ru(bpy)<sub>3</sub>]<sup>2+</sup> on an ITO electrode. *J. Hazard. Mater.* **180**(1–3), 703–709 (2010)
  60. S.K. Ponnaiah, P. Prakash, S. Muthupandian, Ultrasonic energy-assisted in-situ synthesis of RuO/PANI/g-C<sub>3</sub>N<sub>4</sub> nanocomposite: application for picomolar-level electrochemical detection of endocrine disruptor (bisphenol-A) in humans and animals. *Ultrason. Sonochem.* **58**(6), 1–10 (2019)
  61. Y. Si, A.Y. Zhang, C. Liu, D.N. Pei, H.Q. Yu, Photo-assisted electrochemical detection of bisphenol A in water samples by renewable {001}-exposed TiO<sub>2</sub> single crystals. *Water Res.* **157**(28), 30–39 (2019)
  62. M.G. Peleyeju, A.O. Idris, E.H. Umukoro, J.O. Babalola, O.A. Arotiba, Electrochemical detection of 2,4-dichlorophenol on a ternary composite electrode of diamond, graphene, and polyaniline. *ChemElectroChem* **4**(5), 1074–1080 (2017)
  63. J. Zuo, Y. Shen, L. Wang, Q. Yang, Z. Cao, H. Song, Z. Ye, S. Zhang, Flexible electrochemical sensor constructed using an active copper center instead of unstable molybdenum carbide for simultaneous detection of toxic Catechol and Hydroquinone. *Microchem. J.* **187**, 1–10 (2023)
  64. H. Hammani, F. Laghrib, A. Farahi, S. Lahrach, T. El Ouafy, A. Aboulkas, Preparation of activated carbon from date stones as a catalyst to the reactivity of hydroquinone: application in skin whitening cosmetics samples. *J. Sci. Adv. Mater. Dev.* **4**(3), 451–458 (2019)
  65. Y. Liu, Y.M. Wang, W.Y. Zhu, C.H. Zhang, H. Tang, J.H. Jiang, Conjugated polymer nanoparticles-based fluorescent biosensor for ultrasensitive detection of hydroquinone. *Anal. Chim. Acta* **1012**(6), 60–65 (2018)
  66. B.M. Abu-Zied, M.M. Alam, A.M. Asiri, J. Ahmed, M.M. Rahman, Efficient hydroquinone sensor development based on Co<sub>3</sub>O<sub>4</sub> nanoparticle. *Microchem. J.* **157**(27), 1–9 (2020)
  67. H. Wang, R. Li, Z. Li, Nanohybrid of Co<sub>3</sub>O<sub>4</sub> and histidine-functionalized graphene quantum dots for electrochemical detection of hydroquinone. *Electrochim. Acta* **255**(29), 323–334 (2017)
  68. Y. Song, M. Zhao, X. Wang, H. Qu, Y. Liu, S. Chen, Simultaneous electrochemical determination of catechol and hydroquinone in seawater using Co<sub>3</sub>O<sub>4</sub>/MWCNTs/GCE. *Mater. Chem. Phys.* **234**(30), 217–223 (2019)
  69. Y. Liu, H. Liao, Y. Zhou, Y. Du, C. Wei, J. Zhao, Fe<sub>2</sub>O<sub>3</sub> Nanoparticle/SWCNT composite electrode for sensitive electrocatalytic oxidation of hydroquinone. *Electrochim. Acta* **180**(11), 1059–1067 (2015)
  70. Y. Wang, Y. Xiong, J. Qu, J. Qu, S. Li, Selective sensing of hydroquinone and catechol based on multiwalled carbon nanotubes/polydopamine/gold nanoparticles composites. *Sens. Actuators B Chem.* **223**(28), 501–508 (2016)

71. P.S. Ganesh, B.E. Kumara Swamy, O.E. Fayemi, E.S.M. Sherif, E.E. Ebenso, Poly(crystal violet) modified pencil graphite electrode sensor for the electroanalysis of catechol in the presence of hydroquinone. *Sens. Biosens. Res.* **20**(1), 47–54 (2018)
72. A. Anil Kumar, B.E. Kumara Swamy, T. Shobha Rani, P.S. Ganesh, R.Y. Paul, Voltammetric determination of catechol and hydroquinone at poly(murexide) modified glassy carbon electrode. *Mater. Sci. Eng. C* **98**(19), 746–752 (2019)
73. Y. Liu, Z. Zhang, Y. Li, F. Shi, Y. Ai, B. Wang, S. Zhang, X. Zhang, W. Sun, Electrochemical detection of hydroquinone based on marine biomass carbon from shrimp shells as electrode modifier. *Int. J. Electrochem. Sci.* **18**, 1–7 (2023)
74. W. Si, W. Lei, Z. Han, Q. Hao, Y. Zhang, M. Xia, Selective sensing of catechol and hydroquinone based on poly(3,4-ethylenedioxythiophene)/nitrogen-doped graphene composites. *Sens. Actuators B Chem.* **199**(12), 154–160 (2014)
75. Y. Hu, Z. Xue, H. He, R. Ai, X. Liu, X. Lu, Photoelectrochemical sensing for hydroquinone based on porphyrin-functionalized Au nanoparticles on graphene. *Biosens. Bioelectron.* **47**(14), 45–49 (2013)
76. W. Chen, R. Li, Z. Li, Y. Yang, H. Zhu, J. Liu, Promising copper oxide-histidine functionalized graphene quantum dots hybrid for electrochemical detection of hydroquinone. *J. Alloys Compd.* **777**(22), 1001–1009 (2019)
77. X. Ma, J. Chen, Y. Wu, S. Devaramani, X. Hu, Q. Niu,  $\pi$ - $\pi$  nanoassembly of water-soluble metalloporphyrin of ZnTCPP on RGO/AuNPs/CS nanocomposites for photoelectrochemical sensing of hydroquinone. *J. Electroanal. Chem.* **820**(3), 123–131 (2018)
78. S. Radhakrishnan, K. Krishnamoorthy, C. Sekar, J. Wilson, S.J. Kim, A promising electrochemical sensing platform based on ternary composite of polyaniline-Fe<sub>2</sub>O<sub>3</sub>-reduced graphene oxide for sensitive hydroquinone determination. *Chem. Eng. J.* **259**(21), 594–602 (2015)
79. D. Balram, K.Y. Lian, N. Sebastian, Ecofriendly synthesized reduced graphene oxide embellished marsh marigold-like zinc oxide nanocomposite based on ultrasonication technique for the sensitive detection of environmental pollutant hydroquinone. *Ultrason. Sonochem.* **58**(17), 1–13 (2019)
80. H. Wang, Q. Hu, Y. Meng, Z. Jin, Z. Fang, Q. Fu, Efficient detection of hazardous catechol and hydroquinone with MOF-rGO modified carbon paste electrode. *J. Hazard. Mater.* **353**(14), 151–157 (2018)
81. W. Si, W. Lei, Y. Zhang, M. Xia, F. Wang, Q. Hao, Electrodeposition of graphene oxide doped poly (3, 4-ethylenedioxythiophene) film and its electrochemical sensing of catechol and hydroquinone. *Electrochim. Acta* **85**(1), 295–301 (2012)
82. L. Ruiyi, L. Zaijun, W. Guangli, G. Zhiguo, Octadecylamine-functionalized graphene vesicles based voltammetric sensing of hydroquinone. *Sens. Actuators B Chem.* **276**(27), 404–412 (2018)
83. L. Zaijun, S. Xiulan, X. Qianfang, L. Ruiyi, F. Yinjun, Y. Shuping, Green and controllable strategy to fabricate well-dispersed graphene – gold nanocomposite film as sensing materials for the detection of hydroquinone and resorcinol with electrodeposition. *Electrochim. Acta* **85**(30), 42–48 (2012)
84. T. Chen, J. Xu, M. Arsalan, Q. Sheng, J. Zheng, Controlled synthesis of Au@Pd core-shell nanocomposites and their application for electrochemical sensing of hydroquinone. *Talanta* **198**(19), 78–85 (2019)
85. M.S. Tsai, J.C. Lu, P.G. Su, One-pot synthesis of AuNPs/RGO/WO<sub>3</sub> nanocomposite for simultaneously sensing hydroquinone and catechol. *Mater. Chem. Phys.* **215**(21), 293–8 (2018)
86. R. Huang, D. Liao, S. Chen, J. Yu, X. Jiang, A Strategy for effective electrochemical detection of hydroquinone and catechol: decoration of alkalization-intercalated Ti<sub>3</sub>C<sub>2</sub> with MOF-derived N-doped porous carbon. *Sens. Actuators B Chem.* **8**(5), 1–11 (2020)
87. R. Huang, S. Chen, J. Yu, X. Jiang, Self-assembled Ti<sub>3</sub>C<sub>2</sub>/MWCNTs nanocomposites modified glassy carbon electrode for electrochemical simultaneous detection of hydroquinone and catechol. *Ecotoxicol. Environ. Saf.* **184**(27), 1–8 (2019)
88. M. Zhang, J. Ye, P. Fang, Z. Zhang, C. Wang, G. Wu, Facile electrochemical preparation of NaOH nanorods on glassy carbon electrode for ultrasensitive and simultaneous sensing of hydroquinone, catechol and resorcinol. *Electrochim. Acta* **317**(4), 618–627 (2019)
89. P.A. Raymundo-Pereira, A.M. Campos, C.D. Mendonc, M.L. Calegario, S.A. Machado, O.N. Oliveira Jr., Printex 6L carbon nanoballs used in electrochemical sensors for simultaneous detection of emerging pollutants hydroquinone and paracetamol. *Sens. Actuators B Chem.* **252**(27), 165–174 (2017)
90. P.A. Raymundo-pereira, N.O. Gomes, S.A.S. Machado Jr., ONO., Simultaneous, ultrasensitive detection of hydroquinone, paracetamol and estradiol for quality control of tap water with a simple electrochemical method. *J. Electroanal. Chem.* **848**(19), 1–7 (2019)
91. M. Deng, S. Lin, X. Bo, L. Guo, Simultaneous and sensitive electrochemical detection of dihydroxybenzene isomers with UiO-66 metal-organic framework / mesoporous carbon. *Talanta* **174**(22), 527–538 (2017)
92. G. Zhu, Q. Tang, M. Huang, J. Yang, R. Xu, J. Liu, Polyaniline nanocircular array on carbon nano fiber for supersensitive determination of nitrophenol. *Sens. Actuators B Chem.* **320**(12), 1–11 (2020)
93. A. El, F. Galli, L. Moddeur, A. Djadoun, D.C. Bo, Low-cost synthesis of Cu $\alpha$ -Fe<sub>2</sub>O<sub>3</sub> from natural HFeO<sub>2</sub>: application in 4- nitrophenol reduction. *J. Environ. Chem. Eng.* **8**(24), 1–10 (2020)
94. J. Li, L. He, J. Jiang, Z. Xu, M. Liu, X. Liu, Facile syntheses of bimetallic Prussian blue analogues (K<sub>x</sub>M [Fe(CN)<sub>6</sub>]. nH<sub>2</sub>O , M= Ni, Co, and Mn ) for electrochemical determination of toxic 2-nitrophenol. *Electrochim. Acta* **353**, 1–12 (2020)
95. T.W. Chen, U. Rajaji, S.M. Chen, R.J. Ramalingam, Developing green sonochemical approaches towards the synthesis of highly integrated and interconnected carbon nano fiber decorated with Sm 2 O 3 nanoparticles and their use in the electrochemical detection of toxic 4- nitrophenol. *Ultrason. Sonochem.* **58**(9), 1–8 (2019)
96. B. Bhaduri, T. Polubesova, Facile synthesis of carbon-supported silver nanoparticles as an efficient reduction catalyst for aqueous 2-methyl- p -nitrophenol. *Mater. Lett.* **267**(21), 1–4 (2020)
97. P. Wiench, B. Grzyb, Z. González, R. Menéndez, B. Handke, G. Gryglewicz, pH robust electrochemical detection of 4-nitrophenol on a reduced graphene oxide modified glassy carbon electrode. *J. Electroanal. Chem.* **787**(18), 80–87 (2017)
98. C. Li, Z. Wu, H. Yang, L. Deng, X. Chen, Reduced graphene oxide-cyclodextrin-chitosan electrochemical sensor: effective and simultaneous determination of o- and p-nitrophenols. *Sens. Actuators B Chem.* **251**(13), 446–454 (2017)
99. N.I. Ikhsan, P. Rameshkumar, N.M. Huang, Controlled synthesis of reduced graphene oxide supported silver nanoparticles for selective and sensitive electrochemical detection of 4-nitrophenol. *Electrochim. Acta* **192**(3), 392–399 (2016)
100. S. Ma, Y. Wang, H. Yang, Z.L. Xu, Preparation of ultra-stable PFSA-Ag colloid and its application as electrochemical sensor for 4-nitrophenol detection. *Synth. Met.* **260**(20), 1–9 (2020)
101. A. Sangili, M. Annalakshmi, S.M. Chen, P. Balasubramanian, M. Sundrarajan, Synthesis of silver nanoparticles decorated on core-shell structured tannic acid-coated iron oxide nanospheres for excellent electrochemical detection and efficient catalytic reduction of hazardous 4-nitrophenol. *Compos. B Eng.* **162**(27), 33–42 (2019)
102. P. Sebest, L. Fojt, V. Ostatna, M. Fojta, A. Danhel, Electrodeposited silver amalgam particles on pyrolytic graphite in (spectro) electrochemical detection of 4-nitrophenol, DNA and green fluorescent protein. *Bioelectrochemistry* **132**(3), 1–9 (2020)
103. S.A. Hira, M. Nallal, K.H. Park, Fabrication of PdAg nanoparticle infused metal-organic framework for electrochemical and solution-chemical reduction and detection of toxic 4-nitrophenol. *Sens. Actuators B Chem.* **298**(22), 1–12 (2019)

104. C. Zhang, S. Govindaraju, K. Giribabu, Y.S. Huh, K. Yun, AgNWs-PANI nanocomposite based electrochemical sensor for detection of 4-nitrophenol. *Sens. Actuators B Chem.* **252**(9), 616–623 (2017)
105. S.A. Hashemi, S.M. Mousavi, S. Bahrani, S. Ramakrishna, Integrated polyaniline with graphene oxide-iron tungsten nitride nanoflakes as ultrasensitive electrochemical sensor for precise detection of 4-nitrophenol within aquatic media. *J. Electroanal. Chem.* **5**(23), 1–12 (2020)
106. F. Saadati, F. Ghahramani, H. Shayani-jam, F. Piri, M.R. Yaftian, Synthesis and characterization of nanostructure molecularly imprinted polyaniline/graphene oxide composite as highly selective electrochemical sensor for detection of p-nitrophenol. *J. Taiwan Inst. Chem. Eng.* **86**(7), 213–221 (2018)
107. D. Peng, J. Zhang, D. Qin, J. Chen, D. Shan, X. Lu, An electrochemical sensor based on polyelectrolyte-functionalized graphene for detection of 4-nitrophenol. *J. Electroanal. Chem.* **734**(2), 1–6 (2014)
108. B.M. Hryniewicz, E.S. Orth, M. Vidotti, Enzymeless PEDOT-based electrochemical sensor for the detection of nitrophenols and organophosphates. *Sens. Actuators B Chem.* **257**(3), 570–578 (2018)
109. Y. Huang, S. Bai, J. Huang, Y. Ma, Q. Zeng, M. Wang, L. Wang, Simultaneous detection of nitrophenol isomers using an easy-to-fabricate thiophene-based microporous polymer film modified electrode. *Microchem. J.* **153**, 104465 (2020)
110. M. Wang, Y. Liu, L. Yang, K. Tian, L. He, Z. Zhang, Bimetallic metal–organic framework derived FeOx/TiO<sub>2</sub> embedded in mesoporous carbon nanocomposite for the sensitive electrochemical detection of 4-nitrophenol. *Sens. Actuators B Chem.* **281**(136), 1063–1072 (2019)
111. G.G. Gerent, A. Spinelli, Magnetite-platinum nanoparticles-modified glassy carbon electrode as electrochemical detector for nitrophenol isomers. *J. Hazard. Mater.* **330**(9), 105–115 (2017)
112. Q. Wang, R. Li, Y. Zhao, T. Zhe, T. Bu, Y. Liu, Surface morphology-controllable magnetic covalent organic frameworks: a novel electrocatalyst for simultaneously high-performance detection of p-nitrophenol and o-nitrophenol. *Talanta* **219**(15), 1–13 (2020)
113. Z. Liu, J. Du, C. Qiu, L. Huang, H. Ma, D. Shen, Electrochemical sensor for detection of p-nitrophenol based on nanoporous gold. *Electrochem. Commun.* **11**(7), 1365–1368 (2009)
114. H.F. Zhou, S.X. Li, Y.J. Wu, D.J. Chen, Y.H. Li, F.Y. Zheng, W.H. Yu, Nitrogen-doped carbon spheres surface modified with in situ synthesized Au nanoparticles as electrochemical selective sensor for simultaneous detection of trace nitrophenol and dihydroxybenzene isomers. *Sens. Actuators B Chem.* **237**(22), 487–94 (2016)
115. A. Shah, M. Akhtar, S. Aftab, A. Hassan, Gold copper alloy nanoparticles (Au-CuNPs) modified electrode as an enhanced electrochemical sensing platform for the detection of persistent toxic organic pollutants. *Electrochim. Acta* **241**(1), 281–290 (2017)
116. Q. Ding, Z. Kang, L. Cao, M. Lin, H. Lin, D.P. Yang, Conversion of waste eggshell into difunctional Au/CaCO<sub>3</sub> nanocomposite for 4-nitrophenol electrochemical detection and catalytic reduction. *Appl. Surf. Sci.* **510**(25), 1–10 (2020)
117. S.B. Khan, K. Akhtar, E.M. Bakhsh, A.M. Asiri, Electrochemical detection and catalytic removal of 4-nitrophenol using CeO<sub>2</sub>-Cu<sub>2</sub>O and CeO<sub>2</sub>-Cu<sub>2</sub>O/CH nanocomposites. *Appl. Surf. Sci.* **492**(20), 726–735 (2019)
118. E.Y. Danish, E.M. Bakhsh, K. Akhtar, Design of chitosan nanocomposite hydrogel for sensitive detection and removal of organic pollutants. *Int. J. Biol. Macromol.* **159**(8), 276–286 (2020)
119. J. Zhang, S. Cui, Y. Ding, X. Yang, K. Guo, J.T. Zhao, Two-dimensional mesoporous ZnCo<sub>2</sub>O<sub>4</sub> nanosheets as a novel electrocatalyst for detection of o-nitrophenol and p-nitrophenol. *Biosens. Bioelectron.* **112**(12), 177–185 (2018)
120. D. Balram, K.Y. Lian, N. Sebastian, Ultrasound-assisted synthesis of 3D flower-like zinc oxide decorated fMWCNTs for sensitive detection of toxic environmental pollutant 4-nitrophenol. *Ultrason. Sonochem.* **60**(16), 1–11 (2020)
121. V. Anbumannan, M. Dinesh, R.T. Rajendra Kumar, K. Suresh, Hierarchical  $\alpha$ -MnO<sub>2</sub> wrapped MWCNTs sensor for low level detection of p-nitrophenol in water. *Ceram. Int.* **45**(17), 23097–23103 (2019)

**Publisher's Note** Springer Nature remains neutral with regard to jurisdictional claims in published maps and institutional affiliations.